EXPERIMENTAL AND NUMERICAL STUDY OF THE TOOL-PART INTERACTION IN AUTOCLAVED COMPOSITE PARTS

by
Onur YÜKSEL

B.S., Mechanical Engineering, Middle East Technical University, 2012

Submitted to the Institute for Graduate Studies in
Science and Engineering in partial fulfillment of
the requirements for the degree of
Master of Science

Graduate Program in Mechanical Engineering
Boğaziçi University
2015

EXPERIMENTAL AND NUMERICAL STUDY OF THE TOOL-PART INTERACTION IN AUTOCLAVED COMPOSITE PARTS

APPROVED BY

Assoc. Prof. Nuri B. Ersoy . . . . . .
(Thesis Supervisor)

Assoc. Prof. Serdar Soyöz . . . . . .

Prof. Fazıl Önder Sönmez . . . . . .

DATE OF APPROVAL: 22.01.2015

ACKNOWLEGDEMENTS

I would like to express my deepest gratitude to my supervisor Assoc. Prof. Nuri B. Ersoy. He taught me how to question thoughts and express ideas. His patience and support helped me overcome many crisis situations in different projects and research.

I am also thankful to my committee members , Assoc. Prof. Serdar Soyöz and Prof. Fazıl Önder Sönmez for their comments and constructive critics.

I am grateful to my mother, Ayfer Yüksel, my father, Ersin Yüksel and brother, Ali Oğuz Yüksel for their continuous love, encouragement and patience.

I would like to express a special thanks to Assist. Prof. Kenan Çınar for his valuable insights and recommendations besides technical assistance.

I am also grateful to my friends and colleagues Fatih Ertuğrul Öz, Selçuk Hazar, Efe Yamaç Yarbaşı and Farzad Bina for their friendship and helps.

ABSTRACT

EXPERIMENTAL AND NUMERICAL STUDY OF THE TOOL-PART INTERACTION IN AUTOCLAVED COMPOSITE PARTS

Fibre reinforced composite materials cannot be manufactured without any geometric distortions. The aim of this study is to investigate the effect of tool-part interaction on shape distortions in composite manufacturing. A basic Finite Element Model for the chosen geometry and stacking sequences was developed to predict numerically the actual distortion of composite parts. Three step model was implemented to take into account three different states of resin, namely viscous, rubbery and glassy properties. Composite parts in flat and double curvature geometries were manufactured and distortions were measured to compare with the numerical results. In addition to the comparison of distortion between numerical and experimental studies, tool-part interaction was measured experimentally in order to examine the isolated effect of tool part-interaction. The shape distortion measurements were compared with the numerical predictions and the discrepancies were discussed.

ÖZET

OTOKLAV İLE ÜRETİLEN PARÇALARDA KALIP PARÇA ETKİLEŞİMİNİN DENEYSEL VE NUMERİK ÇALIŞMALAR İLE İNCELENMESİ

Sürekli elyaf takviyeli kompozit parçaları geometrik çarpılmalar olmadan üretebilmek mümkün değildir. Bu çalışmanın amacı kompozit parça imalatı sırasında kalıp-parça etkileşiminin çarpılmalar üzerindeki etkisinin incelenmesidir. Kompozit parçaların çarpılmalarının numerik olarak tahmin edilebilmesi için belli parça geometrileri ve serim konfigürasyonları için temel bir Sonlu Eleman Modeli geliştirilmiştir. Oluşturulan 3 adımlı sonlu eleman modeline malzemenin akışkan, lastiksi ve camsı hallerinin özellikleri entegre edilmiştir. Düz ve iki eksende ters eğimli parçalar üretilmiş, bu parçaların çarpılmaları ölçülmüş ve numerik çalışma sonuçları ile karşılaştırılmıştır. Çarpılmaların karşılaştırılmasına ek olarak, kalıp-parça etkileşiminin yalıtılmış etkisinin görülebilmesi için parça ve kalıp arası etkileşim deneysel olarak ölçülmüştür. Çarpılmalara ilişkin nümerik tahminler ölçülen çarpılmalar ile karşılaştırılmış ve aradaki farkların nedenleri incelenmiştir.

TABLE OF CONTENTS

ABSTRACT iv

ÖZET v

LIST OF FIGURES viii

LIST OF TABLES x

LIST OF SYMBOLS xi

LIST OF ACRONYMS / ABBREVIATIONS xii

1. INTRODUCTION 1

1.1. Literature Review 3

1.1.1. Process Induced Residual Stresses 3

1.1.2. Resin Property Development 11

1.1.3. Process Modelling 13

1.2. Problem Statement 15

2. EXPERIMENTAL WORK 17

2.1. Materials and Manufacturing 17

2.2. Specimen Preparation 19

2.3. Measurement of Part Geometry 20

2.4. Tool-Part Interaction Measurements 21

3. FINITE ELEMENT ANALYSIS 23

3.1. Stress Calculation and Development of Constitutive Equation 23

3.2. Steps of Analysis 26

3.3. Tool-Part Interaction 29

3.4. Meshing and Boundary Conditions 30

4. RESULTS AND DISCUSSION 33

4.1. Tool-Part Interaction 33

4.2. Comparison of Observed and Predicted Distortion Fields for Flat Plate Parts 38

4.3. Comparison of Observed and Predicted Distortion Fields for Double Curvature Parts..... 44

5. CONCLUSION AND FUTURE WORKS 49

REFERENCES 52

LIST OF FIGURES

Figure 1.1. Manufacturer Recommended Cure Cycle. 2
Figure 1.2. A reduction in enclosed angle. 4
Figure 1.3. Shear lag phenomena (a) restricted in shear (b) no restriction in shear. .. 7
Figure 1.4. Effect of resin flow on the warpage. 8
Figure 1.5. The effect of tool-part interaction on flat parts. 9
Figure 1.6. The degree of cure and the glass transition temperature progress [44]. . 12
Figure 1.7. Development of mechanical properties through the cure cycle [47]..... 13
Figure 2.1. Vacuumed parts on double curvature tool. 18
Figure 2.2. Bagging arrangement. 18
Figure 2.3. MRCC graph taken from the autoclave screen. 19
Figure 2.4. Schematic representation of vacuum bagging. 20
Figure 2.5. Spot curing setup. 21
Figure 2.6. Strain gage set-up. 22
Figure 3.1. Material coordinate system. 23
Figure 3.2. Stress calculation progress. 26
Figure 3.3. Resin property progress through MRCC. 27
Figure 3.4. Coulomb friction model. 29
Figure 3.5. Double curvature tool and Symmetric BC's for double curvature tool. 31
Figure 4.1. Load versus extension data of the uncured prepreg. 34
Figure 4.2. Raw data and moving average for real time strain data. 35
Figure 4.3. Schematic representation for shear stress on bottom ply. 36
Figure 4.4. Tool-part interaction induced strain [64]. 37
Figure 4.5. Alignment points for tool and scanned data. 38
Figure 4.6. Material orientation for the cross-ply laminate. 39
Figure 4.7. Measured distortion field for [0]4 flat part. 40
Figure 4.8. Finite element results for [0]4 flat parts. 40
Figure 4.9. Deformation of unidirectional plate without Poisson's ratio effect. 41
Figure 4.10. Measured distortion field for [0/90]s flat part. 42
Figure 4.11. Finite element results for [0/90]s flat part. 42

Figure 4.12. Schematic representation of the tool-part interaction in 2-direction. 43
Figure 4.13. Modified distortion field with reduced transverse direction friction coefficient. 44
Figure 4.14. Measured distortion field for [0]4 double curvature part. 45
Figure 4.15. Finite element results for [0]4 double curvature part. 45
Figure 4.16. Cumulative spring in effect of thermal anisotropy, cure shrinkage and tool-part interaction. 46
Figure 4.17. Measured distortion field for [0/90]s double curvature part. 47
Figure 4.18. Finite element results for [0/90]s double curvature part. 47
Figure 4.19. Anisotropic friction coefficient for double curvature cross ply laminate. 48

LIST OF TABLES

Table 2.1. Physical properties of AS4/8552. 19
Table 3.1. Mechanical properties in different steps. 28
Table 3.2. Mesh convergence analysis for double curvature parts. 30
Table 3.3. Mesh convergence analysis for flat parts. 30
Table 3.4. Constraints for symmetric boundary conditions (X: Fixed). 31

LIST OF SYMBOLS

°C	Celsius
E_{11}	Elastic modulus in fibre direction
E_{22}	Elastic modulus in transverse direction
E_{33}	Elastic modulus through thickness
GPa	Gigapascal
Gij	In-plane shear modulus
MPa	Megapascal
mm	Millimeter
Ø	Initial part angle
ΔØ	Total spring-in angle
ΔT	Change in temperature
αii	Coefficient of thermal expansion in principal direction
αØ	Circumferential coefficient of thermal expansion
αR	Radial coefficient of thermal expansion
ε_{11}	Fibre direction strain
ε_{22}	Transverse direction strain
ε_{33}	Through thickness direction strain
$\varepsilon_{ø}$	In-plane chemical shrinkage strain
ε_{R}	Through thickness chemical shrinkage strain
γij	In-plane shear stresses
υij	Poisson’s ratios

LIST OF ACRONYMS / ABBREVIATIONS

AS4/8552	High viscous Prepreg Material
CHILE	Cure hardening instantaneous linear elastic constitutive model
CTE	Coefficient of Thermal Expansion
DMA	Dynamic Mechanical Analyser
DSC	Differential Scanning Calorimeter
FBG	Fibre Bragg Grating
FE	Finite Element
FEM	Finite Element Model
FEP	Fluorinated Ethylene Propylene
FEBM	Finite Element Based Micromechanics
FVF	Fibre Volume Fraction
GIM	Group Interaction Modelling
MRCC	Manufacturer Recommended Cure Cycle
RTM	Resin Transfer Moulding
UD	Unidirectional parts
XP	Cross-ply parts

1. INTRODUCTION

Traditional materials cannot meet the increasing technological demand of users. In order to produce faster, more economical, stronger machines, engineers are looking for new material and manufacturing technologies. Composite materials are one of the most feasible types of emerging material technologies. Although they have been used for years, they are not well known as traditional isotropic materials. Moreover, due to the nature of manufacturing procedures and investment costs, total cost for composite materials is higher than traditional materials. In addition, insufficient information about process parameters and their effects on final products geometry also increase the cost due to scrapped products. These are acceptable cons because composite materials have many favourable properties. On the other hand higher cost is tried to be decreased with considerable research effort in order to strengthen the advantages of composite materials over traditional materials. Despite the lower manufacturing rate, higher possibility of manufacturing defects and higher cost, composite materials are used in various areas like aeronautical, automotive, marine or sporting goods industries due to their superior properties.

Composite materials are non-isotropic materials. Specifically continuous fibre reinforced composite materials are made up of layers which have high elastic modulus and strength in the fibre direction. Designer assembles these layers according to the technical requirements. Parts can be made strong or tough in desired locations, thanks to the versatility of composite materials. Composite materials have high specific moduli in desired directions and have high flexibility in terms of design variety. Controversially, this non-isotropic properties of the layers make manufacturing process considerably more complicated.

Composite fibre reinforced polymers can be manufactured with various methods. Aeronautical parts and especially high technological parts are generally manufactured in autoclaves. An autoclave is a kind of pressure vessel in which temperature and pressure can be controlled. In the autoclave manufacturing technique, prepregs which are prepared from resin impregnated fibre are laid on the mould. Stacking direction is determined according to the design requirements. These lay-ups also known as laminates, are vacuumed in a vacuum bag and heated as stated in Manufacturer Recommended Cure Cycle (MRCC). In MRCC

heat is applied together with pressure. With the help of pressure, voids in resin could be minimized. During the curing process, resin is hardened or toughened by crosslinking of polymer chains. Moreover resin and fibre are bonded chemically. MRCC varies with respect to the chemistry of resin and fibre. An example of MRCC for AS4/8552 prepreg produced by Hexcel could be seen in Figure 1.1.

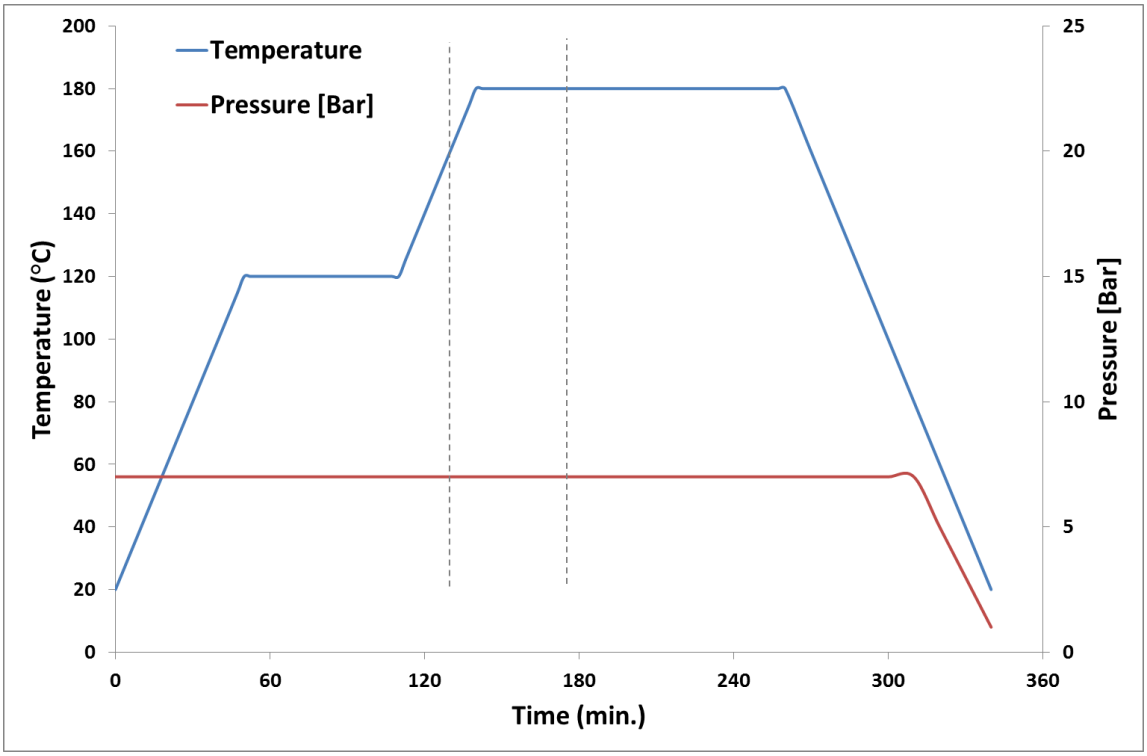


Figure 1.1. Manufacturer Recommended Cure Cycle.

After the curing process, composite parts generally are not exactly of the same geometry as the mould shape. It could be thought as spring back phenomena after bending in isotropic materials. A metallic plate, deformed in a V-shaped mould with some amount of force, will tend to bend in larger angle than V-mould angle after separation. Some amount of energy applied on plate deforms the material and rest of the energy loads the material with stress. After separation, this stress turns into deformation. In the manufacturing process, this phenomena is analogously occurs for composite materials as well. The energy comes from heating in cure cycle. Some amount of energy affects the polymeric structure and the bonds between the fibre and the resin. At the same time, process induced residual stresses are formed by remaining energy. These stresses generally cause distortion. If stress is locked in the part without any deformation, failure limits would change due to the residual stress and

unexpected failures can occur. For composite materials, analysing the source of residual stresses is quite complicated due to different mechanisms involved in micro and macro scales.

The sources of process induced residual stresses at micro scale are (i) Coefficient of thermal expansion (CTE) mismatch between fibres and resin (ii) cure shrinkage and (iii) moisture absorption. At the macro scale, anisotropic incompatibility between different plies and geometric constraints, especially created by tool, are the main sources of residual stress in manufacturing process. Micro scale sources do not lead any large distortion due to self-equilibrating effect. On the other hand, macro scale sources lead large deformations that are not acceptable in most of the applications.

1.1. Literature Review

Increasing popularity of composites raised the necessity to refine the manufacturing technologies for composite materials. This is possible only if the effect of process parameters on final product are understood rigorously. Therefore, in the last decades, process induced residual stresses has attracted much attention from research teams working on composites. Studies with the purpose of refinement in manufacturing of composite materials could be analysed in two main categories. First of them have tried to conceive the sources of process induced residual stresses. Others have focused on prediction of deformations.

1.1.1. Process Induced Residual Stresses

Reasons behind the process induced residual stresses should be comprehended totally in order to control the manufacturing parameters precisely to have a less manufacturing distortions and residual stresses. Hence, considerable research effort has been spent on process induced residual stresses up to now. In this section of the study, different mechanisms in development of the process induced residual stresses will be explained.

Coefficient of Thermal Expansion (CTE) values of fibre and resin are different. Some amount of micro and macro scale residual stresses are caused by this difference. While microscale residual stress does not create any distortion, macroscale does [1]. Due to

different CTEs, effect of temperature changes on fibre and resin dominated directions is different. Generally, CTE of the resin is higher than CTE of the fibre; this means that laminates expand or contract much more in resin dominated directions. In symmetric balanced flat laminates, this phenomena does not lead any macroscale anisotropy, so does not causing any distortion. On the other hand, in curved parts radial direction is resin dominated. Therefore, the thickness direction (radial direction) has lower CTE than the tangential direction. The result of this difference is reduction in the enclosed angle of the laminate as shown in Figure 1. Firstly, Nelson and Cairns have proposed an equation in order to calculate the value of angle reduction due to thermal anisotropy. Initial angle of the part (ϕ), circumferential CTE (α_ϕ), radial CTE (α_R) and temperature change (ΔT) are related to the spring-in angle ($\Delta\phi$) using the following equation:

$$\Delta\phi = \phi.\frac{(\alpha_\phi - \alpha_R).\Delta T}{1+\alpha_R.\Delta T} \tag{1.1}$$

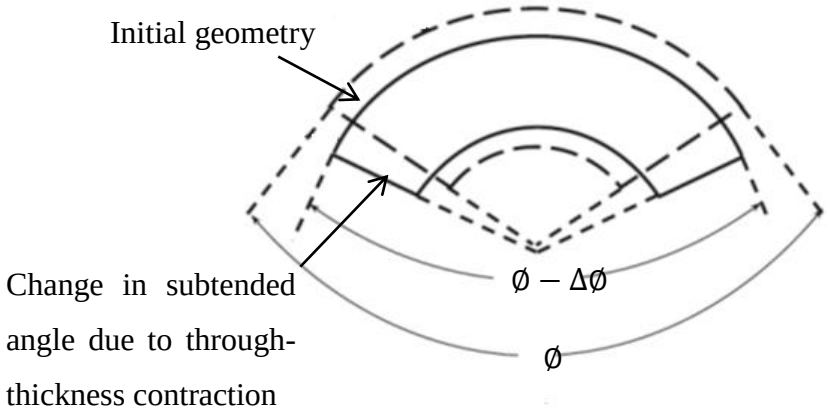


Figure 1.2. A reduction in enclosed angle.

Several researchers [2-5] observed the residual stresses and distortions at some specific points in the cure cycle by interrupted cure technique, which involves fast cooling of the composite part to room temperature at certain points during the MRCC. In this way, variation of transverse CTE and its effect on distortions during cure cycle as well as thermoelastic and non thermoelastic components of distortions can be observed. Gigliotti *et al*. measured the stress free temperature of unbalanced composite samples and they have found that curing temperature is lower than the stress free temperature of samples which are cured beyond vitrification. This outcome shows the existence of non-thermoelastic stress in the part.

Gigliotti *et al*. also found that the change in transverse CTE is negligible below the glass transition temperature and out of plane deformation increase sharply during the second heating ramp. Ersoy *et al*. [5] modified the technique by using it in C-shaped, curved parts. The C-shape parts were cured within an aluminium tube as the mould. Specimens were quenched before and after vitrification and spring-in values were compared. They have found that more spring-in occurred in specimens quenched before vitrification. With respect to their approach, the reason is larger thermal expansion coefficient for the rubbery state, which is stated above the glass transition temperature, than the glassy state. So the parts quenched in rubbery state tend to spring-in more. They have also found that %50 of spring-in is thermoelastic. Different approaches to identify the thermoelastic and non-thermoelastic components of spring-in was proposed by Radford and Rennick [6] and then by Garstka [7]. They have observed the spring-in angle of samples heated in an oven. In these studies, parameters like laminate thickness, stacking sequence and part radius are variable in order to determine the relationship between these parameters and thermoelastic stress. Radford and Rennick [6] have found that stacking sequence affects the thermoelastic component but laminate thickness and corner radius does not. On the other hand Garstka [7] has found that the laminate thickness is related to the thermoelastic component of spring-in due to higher resin percolation and corner thickening.

Cure shrinkage is another mechanism that can cause process induced deformation. In thermoset polymers, chemical cross linking, which makes resin hardened, increases the density so that the volume decreases [8]. Cure shrinkage create strains in thickness direction without any constraint. However, fibres constrain the shrinkage strain in the in-plane directions. Therefore, higher strain rates in thickness direction create the residual stresses in the same way as thermal anisotropy does. Redford and Diefendorf [9] have modified Equation 1.1 with the effect of cure shrinkage term.

They have integrated the in-plane chemical shrinkage strain (ε_{ϕ}) and transverse chemical shrinkage strain (ε_{R}) into Equation 1.1 in the following equation;

$$\Delta\phi = \phi.[\frac{(\alpha_\phi - \alpha_R).\Delta T}{1 + \alpha_R.\Delta T} + (\frac{\varepsilon_\phi - \varepsilon_R}{1 + \varepsilon_R}) \quad (1.2)$$

Chemical cure shrinkage strains were monitored by various researchers with different approaches. A simple method used by White and Hahn [10] measured the thickness change of prepreg plies which are taken from different phases of curing cycle and cooled to room temperature. Volumetric dilatometer [11-14], Thermo-Mechanical Analyser (TMA) [15], Dynamic Mechanical Analyser (DMA) [16] and interlaced camera [7] were all used to measure the cure shrinkage strains. The studies showed that cross ply laminates have more cure shrinkage in thickness direction than the unidirectional laminates. In cross ply laminates, fibres constrain the resin cure shrinkage in both in-plane directions and volume reduction is compensated by higher through-the-thickness strain.

Wisnom *et al*. enhanced the analytical approach which was mentioned in Equation 1.2. Wisnom *et al*. have shown that low shear modulus of resin at rubbery state causes shear lag between sequential plies. This phenomena results in lower spring-in angles than values calculated Equation 1.2. Shear lag phenomena was also embedded in a two-step FEM model [17]. The results of FEM model matches the analytical approach developed by Wisnom *et al*. [18]. To conclude, thicker laminates are manufactured with less spring-in angles due to the existence of shear lag phenomena which can be seen in Figure 1.2 schematically. This phenomena caused by low shear modulus of resin which allows some shear deformation (shear-lag) between plies to maintain the same arc length. This mechanism decreases the amount of in-plane stress and causes smaller spring-in values.

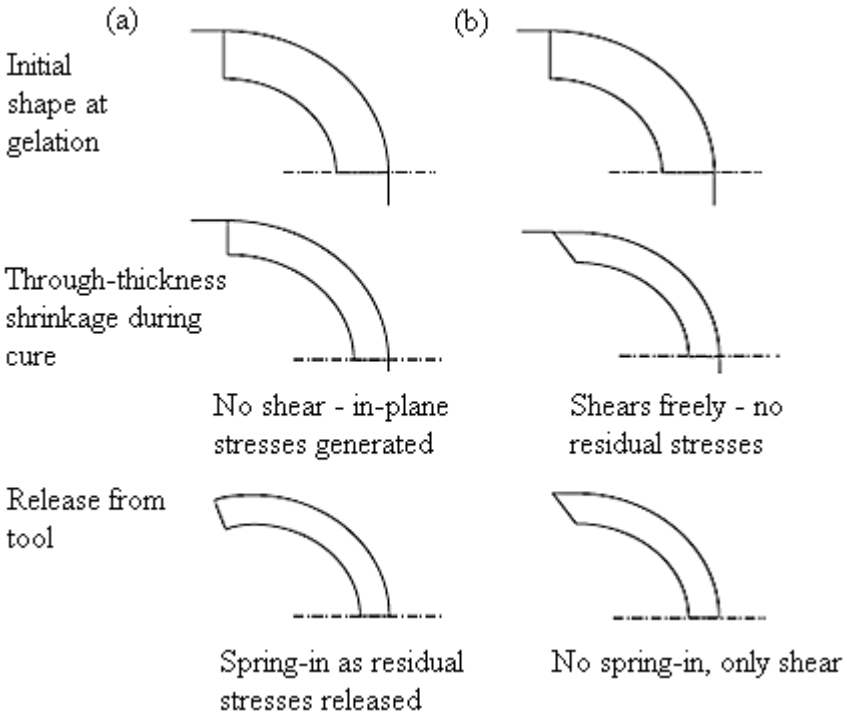


Figure 1.3. Shear lag phenomena (a) restricted in shear (b) no restriction in shear.

Thermal anisotropy and cure shrinkage causes process induced residual stress especially in curved parts. On the other hand, there are also different mechanisms which cause out-of-plane distortions for flat parts. For example, resin flow creates the fibre volume fraction gradient which results out-of-plane distortions due to mechanical property gradients along the thickness [19]. Void distribution is affected by resin flow and resin pressure distribution which is directly related to resin flow.

Bleeders that cover the laminate under the vacuum bag are used to obtain higher Fibre Volume Fraction (FVF) for higher specific strength. It sucks the excessive resin from the bag side of the laminate at liquid state. Therefore FVF gradient is formed along the thickness direction. Laminates have higher FVF at the bag side and lower FVF at the mould side. In other words parts manufactured with bleeder have higher CTE at the mould side than the bag side. During the cool down phase of MRCC, shrinkage strains are getting larger through the thickness direction from bag side to the mould side. This phenomenon results in warpage for flat parts. The mechanism can be seen schematically in Figure 1.4.

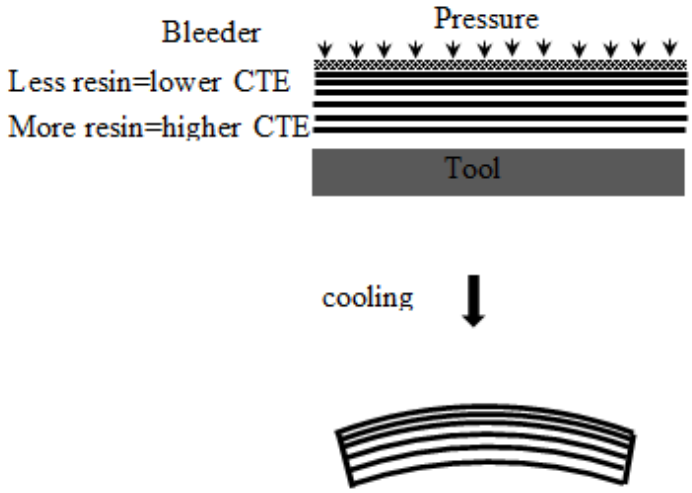


Figure 1.4. Effect of resin flow on the warpage.

Various research papers have been published on prediction of resin flow in autoclave processes [15, 20-25]. The main focus point of these papers is the consolidation of laminates of simple shapes. Different approaches about modelling of flow and compaction have been developed in these studies.

Classical laminate plate theory does not take into account the FVF gradients in composite laminates. Darrow [26] studied symmetric carbon fibre/epoxy laminate and proposed to embed the FVF gradient into the classical laminate theory for this material. FVF along the thickness was measured. As expected, Darrow has found that resin-rich regions are located adjacent to the tool and resin-poor regions are located adjacent to the bleeder, most of the middle regions have uniform FVF. Volume fractions were observed as 0.52, 0.57, 0.59 for bleeder side, mid region, and tool side respectively. Finally, mid-plane curvatures were predicted with classical laminate theory which was modified to take into account FVF variations. Darrow showed that the predicted results match the experimental observations.

Another mechanism that causes process induced residual stresses in composite materials is tool-part interaction which is also results in out of plane deformations for flat parts. Tool-part interaction occurs basically due to the CTE difference between the tool and the part. Autoclave pressure applies force to the part on the tool as a normal force, and shear interaction between the part and the tool develops when both of them are subjected to a temperature ramp in MRCC. Shear modulus of the laminate is very low at the beginning of

curing cycle so bag side plies are not stretched due to the tool expansion whereas tool side plies, especially fibres adjacent to the tool are stretched by the tool due to friction between them. Therefore, non-uniform stress distribution is formed in the laminate and locked in while resin is being cured. This phenomenon could be seen schematically in Figure 1.5.

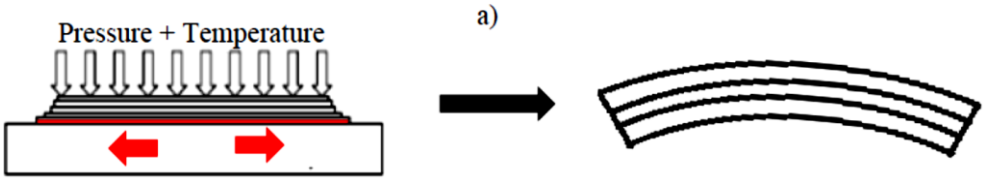


Figure 1.5. The effect of tool-part interaction on flat parts.

Many studies have focused on tool-part interaction and have examined the relationship between warpage and the effect of this interaction [27, 28-41]. Twigg *et al*. [28-30] investigated the effect of tool-part interaction with experimental and numerical methods. An instrumented tool method has been developed in order to understand the interaction mechanism between the tool and the part. An aluminium sheet is placed between the tool and the part. Strain of this aluminium sheet which is caused by tool-part interaction is measured with the help of a strain gage. The results show that sliding friction condition prevails during the heating phases of MRCC. Increasing degree of cure enhances the shear stress. During the holding and cooling periods of MRCC, sticking interface condition prevails. Then, effects of two different release materials, namely, FEP (fluorinated ethylene propylene) and release agent have been examined by Twigg *et al*. It was found that release agent builds up adhesive bonding between tool and part as opposed to release film which prevents the sticking condition. An experimental study conducted by the same group [29] shows that part aspect ratio is more dominant on final warpage than pressure and tool surface condition.

Gartska *et al*. [7] modified the approach of Twigg *et al*. [28-29] by mounting the strain gage on the prepreg with a technique called “spot curing”. A small portion of prepreg, on which strain gage will be attached, was cured with an apparatus in order to provide appropriate bonding surface for strain gage. After calibration of strain gage on uncured

prepreg, laminate was processed following the MRCC. During the process, real time strain data was recorded. Fibre optic sensors (Fibre Bragg Grating Sensors) were also used to measure strains in the laminate during the process [61, 61, 63]. It should be noted that Fibre Bragg Grating (FBG) sensors cannot measure strain for viscous state of the resin in contrast with the instrumented tool and spot curing technique.

Some of the studies on tool-part interaction have focused on simulating the autoclave process with experimental setups in order to examine the friction coefficient and shear stress between tool and part [35-36, 42-44]. Temperature controlled slabs are used to simulate the temperature changes in addition to spring screw system [44] or pneumatic rams that are used to simulate the pressure applied during the MRCC. A tensile testing machine pulled one prepreg layer through the laminate which is heated and pressurized in experimental setup. Load vs. displacement data have been recorded directly from the tensile testing machine. Shear stresses at tool-part interface as a function of pressure and temperature were measured in the study of Ersoy *et al*. [44]. It was shown that even at the beginning of cure cycle, shear stress develop due to the fibre friction. Martin *et al*. and Flanagan *et al*. concluded that tool-part interaction is changing as curing process is advancing. Static friction coefficient has been measured by Martin *et al* and Flanagan *et al*. Kaushik and Raghavan have quantified dynamic friction coefficient together with static friction coefficient, and in order to explain the changes in measured static and dynamic friction coefficients during the process, degree of cure (α) has been taken into account as well as the temperature and the pressure as process variables. The outcomes showed that at the first part of the curing process (α=0.2) static and dynamic friction coefficients drop, as degree of cure increases to α=0.4 both friction coefficients increase, between 0.4-0.6 they decreases and the rest of curing dynamic friction coefficient is constant however static friction coefficient increases considerably. This trends show that interaction between the tool and the part transforms from sliding to sticking condition as the degree of cure increases.

Numerical studies have been conducted on tool-part interaction besides the experimental studies [7, 15, 40-41, 42, 45]. The tool-part interaction is described in [15, 40, 45] as a cure hardening elastic shear layer, in [7, 34, 42] as a sliding friction and in [41] as the part sticks to the tool and expands together. Experimental results are compared to the results of these numerical studies and models are calibrated with respect to the experimental outcomes. In the studies which used elastic shear layer model, stress state at tool part

interface could be described accurately by adjusting the properties like shear modulus and elastic modulus at shear layer. Shear stress distribution is crucial to handle precise distortion prediction with a parametric study [30]. Shear layer assumption was used in a closed form solution for deformations and process induced stresses in the study of Arafath *et al*. [37, 38]. Friction was modelled as Coulomb friction model in the studies of Flanagan [42] and Hubert [46]. In Coulomb friction model, friction coefficient is constant up to a critical shear stress level, after critical shear stress, surfaces start to slip with a constant shear stress.

Other mechanisms like fibre bridging or fibre wrinkling can create process induced residual stresses in composites [56, 59, 60]. However their effect have been ignored for the geometry used in this study.

1.1.2. Resin Property Development

Curing cycle changes the chemical structure of the thermosetting resin. Thermosetting resin contains monomers, and curing process transform monomers into cross-linked polymers. Degree of cure, α, is used to quantify the curing level of resin. Differential Scanning Calorimeter (DSC) method which characterizes the chemical conversion with the heat flow with respect to temperature, could be used to measure the degree of cure. Besides curing, glass transition temperature (T_g) is also important to characterize the resin property. At the glass transition temperature, resin starts to transform from the rubbery to the glassy state. Degree of cure and glass transition temperature progress of AS4/8552 [50], used in this study, can be seen in Figure 1.6.

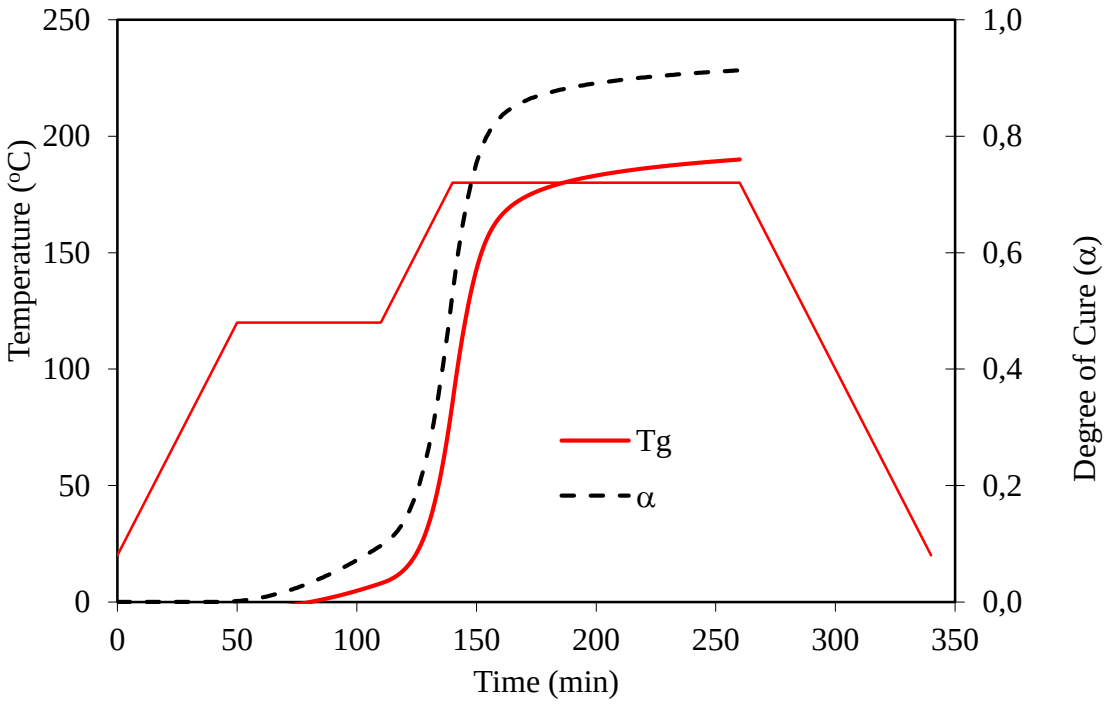


Figure 1.6. The degree of cure and the glass transition temperature progress [44].

Degree of cure rises sharply during the second ramp which indicates the transformation of the resin from a viscous liquid to a rubbery solid. At 45 minutes after the beginning of the second hold period, glass transition temperature is equal to the process temperature. This point is called vitrification point at which resin transforms from a rubbery to a glassy solid [44].

Mechanical behaviour of the resin used in AS4/8552 was observed through cure cycle with an experimental setup, like setups used for investigations of tool-part interaction [35-36,42-44]. Cure cycle conditions were simulated in experimental setup, in which mechanical compression is supplied with heated platens. However this time, tensile testing machine is used to pull one ply through other plies in order to observe interlaminar shear stress during the cure cycle. Results show that shear stress increase sharply at around 160^0C. Sharp increase indicates that resin gelled and started to sustain mechanical loads at 160^0C corresponds to a degree of cure of 0.3.

Ersoy *et al*. [47] used analytical, experimental and numerical methods in order to clarify mechanical properties of AS4/8552 during the cure cycle. Dynamic Mechanical Analyser (DMA) was used to find shear modulus, G_{23} and findings were compared to the

predictions from Group Interaction Modelling (GIM). With the help of mechanical properties of AS4 carbon fibres taken from manufacturer's data sheet, Self-Consistent Field Micromechanics Model (SCFM) and Finite Element Based Micromechanics Model (FEBM) were used to find resin dominated elastic modulus E_{22} in addition to shear moduli G_{12} and G_{23}. In Figure 1.7, the evaluation of resin shear modulus, resin dominated elastic modulus and shear moduli for AS4/8552 can be seen.

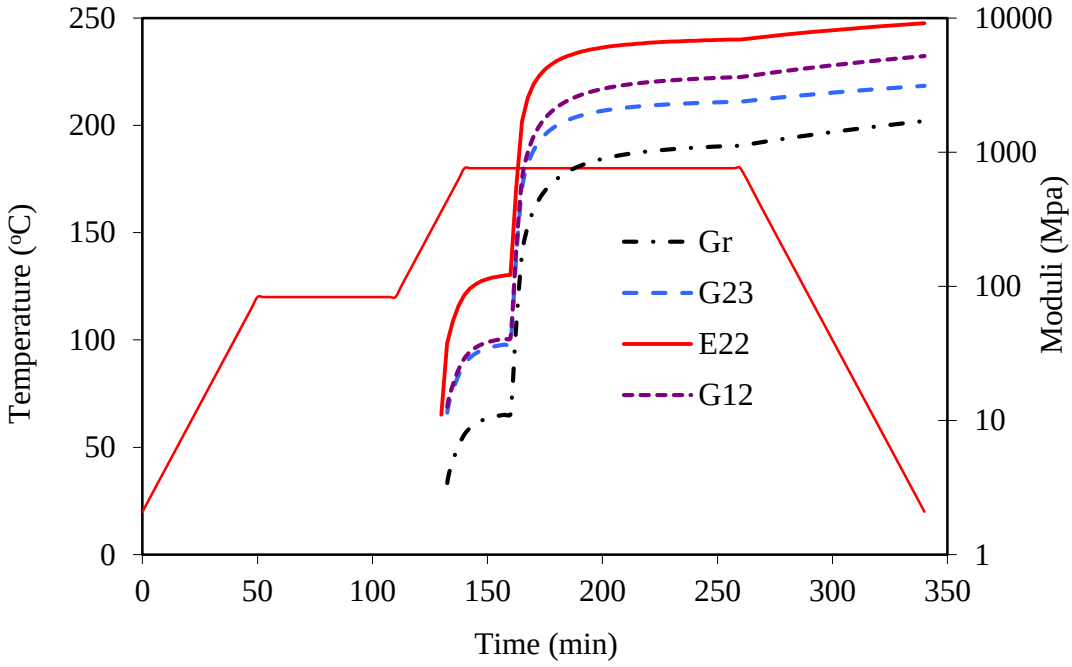


Figure 1.7. Development of mechanical properties through the cure cycle [47].

1.1.3. Process Modelling

For several years, great effort has been devoted for modelling process induced stresses and deformations. One of the first examples in analysing the residual stress development in composites is presented by Hahn and Pagano in [48]. Laminated Plate Theory was used in this study for only cool down period and it was one dimensional. Later, advanced models were developed in order to cover the effects of different mechanisms in different periods of the process [10, 15, 49, 50].

Equation 1.1 was developed by Radford and Diendorf [9] in order to find the thermoelastic deformations of a corner section made of composite materials. Only the effect of temperature change, CTE and initial geometry were taken into account in Equation 1.1. In Equation 1.2, former equation was improved by including the cure shrinkage effect on non-thermoelastic component of deformations [6]. Tool-part interaction and FVF gradient as well as cure shrinkage create non-thermoelastic distortion in composite parts. Thermoelastic and non-thermoelastic portions could be separated with reheating technique. The result obtained by Radford and Rennick [6] showed that non-thermoelastic contribution is more essential than thermoelastic one.

For curved parts, effect of the mould angle on deformation is investigated by Huang and Yang [51]. They have conducted experiments by varying enclosed angles and they have found that spring-in is decreasing as part angle is increasing. Salomi *et al*. [52] have used equation 1.2 in thermoplastic composites and found that fibre distortion at the corner which is not included in Eq. 1.2 creates the difference between experimental and analytical results. Yoon and Kim [53] used 2-D thermoelastic model to examine the effect of cure shrinkage and thermal anisotropy on process induced residual stresses. They have compared experimental results to predicted values from numerical approach in which mechanical properties of lamina were changed with respect to the temperature. Finally it was concluded that chemical cure shrinkage and CTE difference between in-plane and radial directions are mainly responsible from spring-in.

Throughout the manufacturing process, resin is in three different states which can be classified as viscous, rubbery and glassy states. In viscous state, resin is free to flow due to low viscosity. Hubert *et al*. [22] and Min *et al*. [54] have modelled the resin flow with two dimensional flow model. Darcian flow theory could be used for the porous media of fibres. Resin was modelled as an incompressible Newtonian fluid.

In the study of Ersoy *et al*. [17], manufacturing process and the development of process induced stresses and deformations were modelled by a 2-D FEM model. Due to complicated development of material properties along the process, they have simplified the mechanical properties with a 2-step model that included constant properties for rubbery and glassy states. The stresses developed in viscous state of resin were not included to the model. At the first step, resin was modelled as a rubbery material. Then at the second step, it was modelled as a glassy material. Properties of resin in the rubbery step were calculated by GIM (Group

Interaction Modelling). Mechanical properties of the laminate were calculated with two different methods, namely, Finite Element Based Micromechanics and Self Consistent Field Micromechanics. On the other hand mechanical properties for the glassy state were predicted numerically and also measured experimentally. The outcomes of predictions and experiments matched very well with each other [47]. The mechanisms generating stress at the viscous state of resin were ignored in their analysis. A composite tool made of the same material as the part was preferred to make the tool-part interaction minimum. The deformation predictions which has been calculated by the two-step 2D model in this study was very close to the actual deformations. In addition, results showed that spring-in values decreases with increasing thickness which agrees with shear-lag phenomena proposed by Wisnom *et al*. [18].

1.2. Problem Statement

Fibre reinforced composite materials could not be manufactured without any geometric distortions. Parts are never in the exact shape of the moulds which are manufactured according to the nominal geometry of the part. Therefore, designers modify mould geometry, in order to compensate these distortions and obtain desired final geometry. Traditionally, manufacturers try to reach optimal mould design with trial and error approach. However, considering the high costs of the moulds, it is a very expensive approach especially for large parts used in aerospace industry. Moreover, trial and error approach basically ignore the reasons behind the problem which engineers should solve in order to increase the accessibility of composite materials.

The sources of process induced residual stresses are hard to analyse due to mutually interactive effects. Sources can also be classified as intrinsic and extrinsic sources. Intrinsic sources depend on material characteristics. Cure shrinkage, CTE mismatch between matrix and fibre are some of the intrinsic sources of process induced residual stresses. Observing the individual effect of each intrinsic source is a challenging issue. In contrast, it is easier to observe the effect of extrinsic sources on process induced residual stresses. It is feasible to

follow a methodology that focuses on extrinsic sources first, and then developing decisive approaches to understand the effect of each individual source.

This study aims to observe the effect of tool-part interaction on shape distortions in composite manufacturing. Spot curing technique is applied to monitor the real time shear stress data on the part due to tool-part interaction. Then, a semi-inverse method which focuses on distortions of final geometry is applied with the help of a Finite Element Model (FEM). Overall distortion of the parts is observed by using 3D scanner. Point clouds that come from 3D scanner are compared with the FE results. When the contribution of tool-part interaction and geometry dependent sources on overall distortion are eliminated, the effects of intrinsic sources could be seen distinctively. Overall distortion field of the double curvature parts were examined and compared with 3-D three step finite element model results. Measured distortion patterns allow us to assess the contribution of different mechanism in numerical study. Therefore, the approach of the finite element model is enhanced by the outcomes of this study.

Effect of tool-part interaction is investigated in this study with plate-shaped parts, which is quite novel, since only strip-shaped parts are used in literature. Using plate-shaped parts allows one to assess the tool-par interaction both in the fibre and transverse directions, as well as the mutual effect of the interactions in two directions. A complex shaped tool with double curvature is also used in this study, a geometry which can be encountered in real aerospace parts, but not used in validation studies before in the literature. This geometry allows one to assess the relative contribution of extrinsic and intrinsic sources of shape distortions in composite materials.

2. Experimental Work

Experimental measurements are essential parts of semi-inverse numerical studies. The verification of numerical models should be done with experimental results. In order to verify the validity of 3D FEM model used in this study, several experiments were carried out. Firstly, composite parts in flat and double curvature geometries were manufactured and distortions were measured to compare to numerical results. In addition to overall comparison of distortion between numerical and experimental studies, tool-part interaction was measured experimentally by strain gages attached on the part in order to examine the isolated effect of tool-part interaction.

2.1.Materials and Manufacturing

Flat plate and double curvature parts were cured on a steel tool which is made of IMPAX P20 hot work tool steel. CTE of tool material is 12.6 μm/m^{0}C. All parts were 300x300mm dimensions. Totally twelve samples were manufactured as three different samples for two different geometries and configurations. Both flat plates and double curvature parts were manufactured in unidirectional $[0]_4$ and cross ply $[0/90]_{2s}$ stacking sequences. Manufacturing processes were carried out in an autoclave with a depth of 1500 mm and inner diameter of 1200 mm. Autoclave used for experiments is capable to increase inner temperature to 400 ^{0}C and inner pressure to 10 Bar. In Figure 2.1, vacuumed parts on double curvature tool can be seen as prepared to be autoclaved.

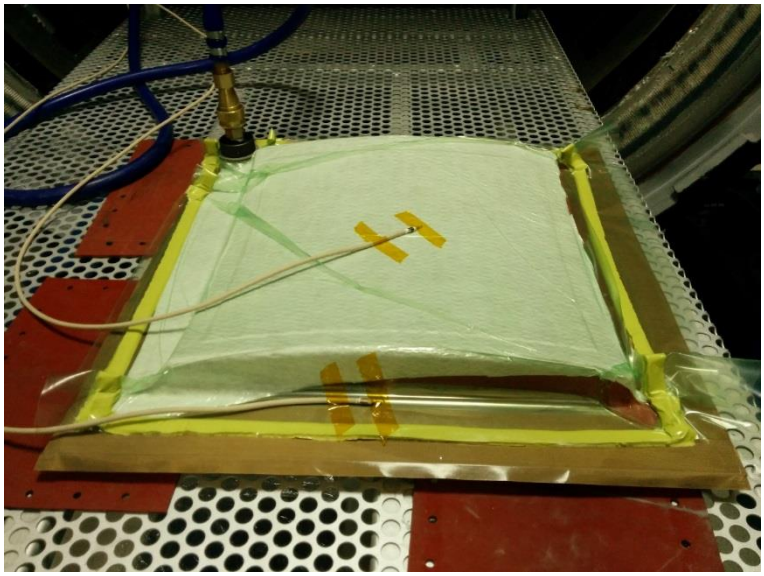


Figure 2.1. Vacuumed parts on double curvature tool.

The vacuum bagging is shown in Figure 2.2, where one layer of peel ply was placed on the top of the prepreg stack. A breather was used on the peel-ply to absorb any excess resin that bled from the laminate. Then a vacuum bag and a sealant tape were applied to seal the whole stack.

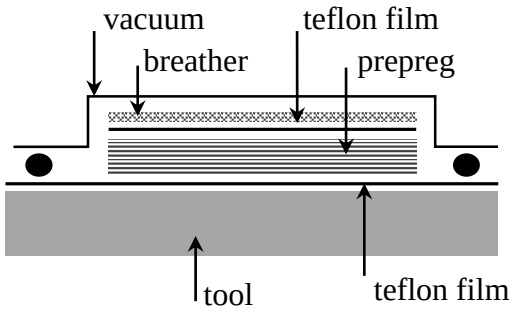


Figure 2.2. Bagging arrangement.

Parts in both geometries were manufactured with carbon epoxy unidirectional prepregs which is supplied by Hexcel Composites with AS4/8552 designation. One ply of uncured prepreg has 0.184 mm thickness and 0.574 nominal fibre volume fraction.

Five step curing cycle is recommended by the manufacturer. According to the Manufacturer's Recommended Cure Cycle (MRCC), lay-up is heated up to 120^0C with a heating rate of 2^0C/min and held there for 1 hour, then it is heated up again to 180^0C with a

heating rate of 2^0C/min and held there for another 2 hours. Finally, part is cooled down to the room temperature with a cooling rate of 2^0C/min. Autoclave is pressurized to 7 bar during the whole curing process and part is vacuumed from the beginning of the process to the middle of the second heating zone. Graph of the MRCC used in experiments which is photographed from the screen of autoclave can be seen in Figure 2.3.

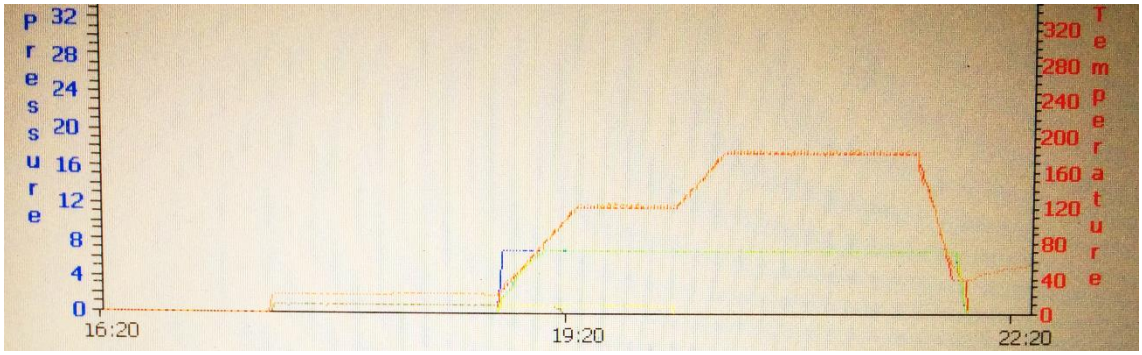


Figure 2.3. MRCC graph taken from the autoclave screen.

Physical properties of AS4/8552 can be seen at Table 2.1.

Table 2.1. Physical properties of AS4/8552.

Fibre Density	1.79 g/cm^3
Resin Density	1.30 g/m^3
Nominal Cured Ply Thickness	0.184 mm
Nominal Fibre Volume	57.42%
Nominal Laminate Density	1.58 g/cm^3

2.2. Specimen Preparation

Surface of the tool in contact with the part is covered with glass fibre reinforced Teflon film in order to remove cured parts easily. Lay-up process was applied carefully for double curvature parts. Due to the geometry of double curvature (DC) tool, it is really hard to

eliminate the misalignment of fibres. During the sample preparation, prepregs were laid up identically over the DC tool. In other words, laying up was started from the same edge of the tool for all of the DC parts. In this way, process induced residual stresses which were caused by fibre misalignment were similar for each part. After laying up process, parts are covered with Teflon film or silicon sheet. Teflon film cannot take the shape of double curvature geometry without wrinkles, so it cannot be used for double curvature parts. On the other hand, smooth upper surface can be obtained with silicon film. Then, breather fabric and vacuum bag cover them all. Breather fabric is used to obtain uniform vacuum and pressure distribution. Vacuum bag is sealed with a heat resistant sealant tape. After bagging, vacuum with magnitude of 0.9 bar is applied to the laminate in order to remove entrapped air. Finally, laminate is made ready to be processed through MRCC.

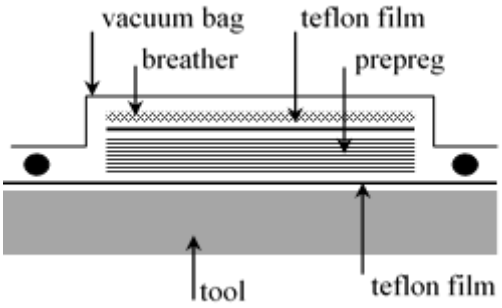


Figure 2.4. Schematic representation of vacuum bagging.

2.3.Measurement of Part Geometry

The deformation field of manufactured parts were obtained by METRIS MCA II 7 axis laser scanner. 3-D scanner was used for taking point clouds of parts in their final geometries. These point clouds compared with tool geometries in RAPIDFORM XOV software. Deformed shape of parts was virtually placed on tool. A colour map which shows vertical distance between the point cloud and tool surface is provided by software. Additionally, comparison of linear sections through different directions is substantial to examine the difference between flat and curved parts. For double curvature parts

deformation patterns indicate the effect of cure shrinkage and thermal anisotropy on warpage.

Manufactured parts are 4 ply laminates, means that weight can cause out of plane deformations. Therefore, parts were hanged from the edge perpendicular to the fibre direction so gravitational deformations were minimized during the scanning process. Tool side surfaces were scanned in order to minimize roughness.

2.4.Tool-Part Interaction Measurements

Due to the higher CTE and friction between the tool and the part, the tool exerts shear stress on the tool side of the part. Strain gages can be used to observe this shear stress directly. Uncured prepreg surface is not convenient to mount a strain gage on it. Different methods have been developed to deal with this problem. For example, Gartska [7] have used instrumented ply technique in which strain gage was mounted directly on prepregs. In this study, spot curing technique was used to provide a convenient mounting surface. A small spot on prepreg was cured by a device which is designed for this purpose. Schematic demonstration of spot curing setup can be seen in Figure 2.5.

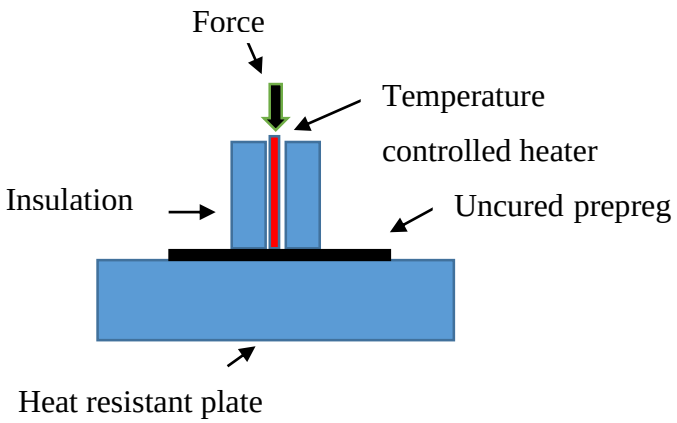


Figure 2.5. Spot curing setup.

In the spot curing setup, a resistance heater and a thermocouple are mounted on the tip of a metallic cylinder which is covered with thick hollow Teflon housing for isolation. Heater is controlled by a PID controller. Prepreg cures slowly even at room temperature so in order to

complete spot curing process with maximum possible degree of cure at the cured spot and minimum around the spot, heater temperature at the tip is set to reach to 240°C at 30 s, and held there for 240°C for 10 minutes. During this process, strain gage is bonded to the cured spot of the prepreg by the epoxy resin of the prepreg itself.

Another one ply sample with spot curing was prepared for tensile testing. Glass fibre tabs were attached to the tips of uncured ply and sample was loaded quasi-statically while force and strain data were acquired simultaneously. Data taken from the strain gage during the curing process was calibrated with the load-strain diagram obtained from tensile testing of the uncured ply.

Strain gage measurement were done with quarter bridge type to arrangement. A dummy gage mounted on a cured laminate in the fibre direction is placed in the autoclave as a temperature compensation gage. Schematic view of strain gage in autoclave can be seen Figure 2.6.

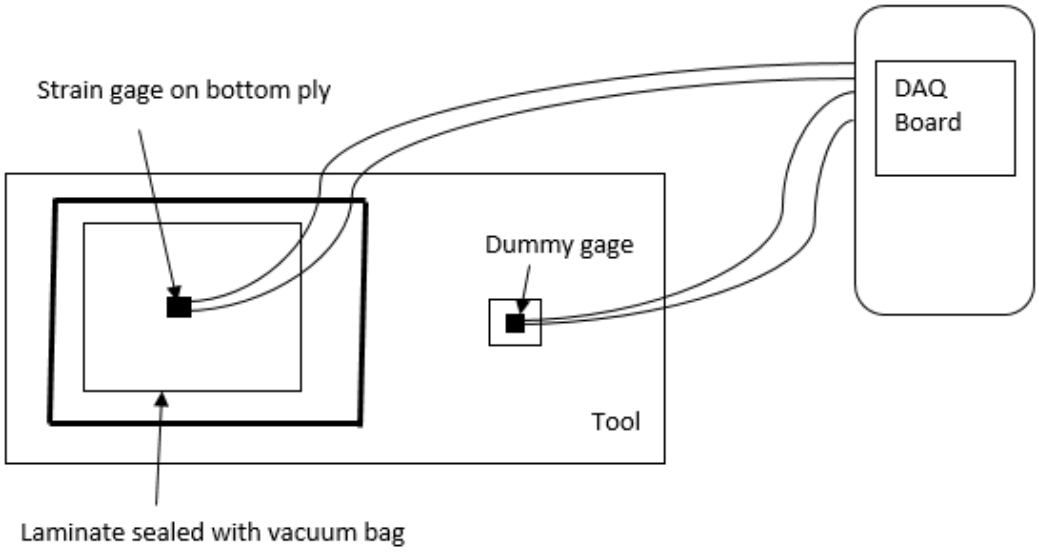


Figure 2.6. Strain gage set-up.

3. Finite Element Analysis

A basic FE model for the geometry and stacking sequences used in this study was developed to predict the actual distortion of composite parts. 3-step model was implemented to take into account three different states of resin, namely viscous, rubbery and glassy properties. The mechanical properties of resin are assumed to be constant in each step. Properties are changed at gelation and vitrification points, at 30% degree of cure and 70% degree of cure respectively [17]. Mechanical properties for viscous, rubbery and glassy states are embedded to the ABAQUS Model. Cure Hardening Instantaneously Linear Elastic (CHILE) model was used to develop constitutive equations which are explained in the next section [57].

3.1.Stress Calculation and Development of Constitutive Equation

Continuous fibre reinforced composite materials are orthotropic materials because of this material coordinate systems are defined according to the fibre direction. In order to standardize the material coordinate systems for composite materials, 1-direction is used for fibre direction, 2-direction for transverse direction and 3-direction for through-thickness direction. Material coordinate system can be seen in Figure 3.1.

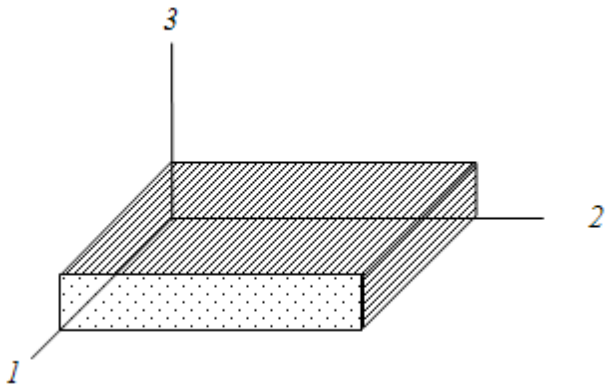


Figure 3.1. Material coordinate system.

Constitutive equation for the composite materials is shown in Equation 3.1.

$$\begin{Bmatrix} \sigma_1 \\ \sigma_2 \\ \sigma_3 \\ \sigma_{23} \\ \sigma_{31} \\ \sigma_{12} \end{Bmatrix} = \begin{bmatrix} \frac{(1-v_{12}v_{31})}{E_1E_3\Delta} & \frac{(v_{12}+v_{32}v_{13})}{E_1E_3\Delta} & \frac{(v_{13}+v_{12}v_{23})}{E_1E_2\Delta} & 0 & 0 & 0 \\ \frac{(v_{12}+v_{32}v_{13})}{E_1E_3\Delta} & \frac{(1-v_{12}v_{31})}{E_1E_3\Delta} & \frac{(v_{23}+v_{21}v_{13})}{E_1E_2\Delta} & 0 & 0 & 0 \\ \frac{(v_{13}+v_{12}v_{23})}{E_1E_2\Delta} & \frac{(v_{23}+v_{21}v_{13})}{E_1E_2\Delta} & \frac{(1-v_{12}v_{21})}{E_1E_2\Delta} & 0 & 0 & 0 \\ 0 & 0 & 0 & G_{23} & 0 & 0 \\ 0 & 0 & 0 & 0 & G_{31} & 0 \\ 0 & 0 & 0 & 0 & 0 & G_{12} \end{bmatrix} \begin{Bmatrix} \varepsilon_1 \\ \varepsilon_2 \\ \varepsilon_3 \\ \varepsilon_{23} \\ \varepsilon_{31} \\ \varepsilon_{12} \end{Bmatrix} \quad (3.1)$$

where $\Delta = (1- \nu_{12}\nu_{21}- \nu_{23}\nu_{32}- \nu_{13}\nu_{31}-2\nu_{21}\nu_{32}\nu_{13})/(E_1E_2E_3)$, $G_{23}=E_2/2(1+\nu_{23})$, and $\nu_{12}=\nu_{13}$, $E_2=E_3$, $G_{12}=G_{13}$ for transversely isotropic composites.

Sum of the thermally induced strains ε_j^{th}, mechanically induced strains ε_j^{m} and chemically induced strains ε_j^{ch} is equal to the overall strain in a layer ε_j^{t}.

$$\varepsilon_j^t = \varepsilon_j^{ch} + \varepsilon_j^{th} + \varepsilon_j^m$$

$$\varepsilon_j^m = \varepsilon_j^t - \varepsilon_j^{th} - \varepsilon_j^{ch} \quad (3.2)$$

Using constitutive equation the stresses in a layer calculated by (3.3)

$$\sigma_i = \sum_{j=1}^{6} C_{ij}\,\varepsilon_j, \qquad i = 1\ to\ 6$$

(3.4)

where C is the stiffness matrix.

For the incremental stress tensor Jacobian matrix is used to relate incremental strains to incremental stresses

$$\Delta\sigma_i = \sum_{j=1}^{6} J_{ij}\,\Delta\varepsilon_j^m, \qquad i = 1\ to\ 6$$

where Jacobian matrix for the viscous state is given by

(3.5)

$$J = \begin{bmatrix} E_1 & 0 & 0 & 0 & 0 & 0 \\ 0 & E_2 & 0 & 0 & 0 & 0 \\ 0 & 0 & E_3 & 0 & 0 & 0 \\ 0 & 0 & 0 & 2G_{23} & 0 & 0 \\ 0 & 0 & 0 & 0 & 2G_{31} & 0 \\ 0 & 0 & 0 & 0 & 0 & 2G_{12} \end{bmatrix},$$

(3.6)

for the rubbery and the glassy state Jacobian matrix is calculated with the material properties for each state and given by,

$$J = \begin{bmatrix} \frac{(1-v_{12}v_{31})}{E_1E_3\Delta} & \frac{(v_{12}+v_{32}v_{13})}{E_1E_3\Delta} & \frac{(v_{13}+v_{12}v_{23})}{E_1E_2\Delta} & 0 & 0 & 0 \\ \frac{(v_{12}+v_{32}v_{13})}{E_1E_3\Delta} & \frac{(1-v_{12}v_{31})}{E_1E_3\Delta} & \frac{(v_{23}+v_{21}v_{13})}{E_1E_2\Delta} & 0 & 0 & 0 \\ \frac{(v_{13}+v_{12}v_{23})}{E_1E_2\Delta} & \frac{(v_{23}+v_{21}v_{13})}{E_1E_2\Delta} & \frac{(1-v_{12}v_{21})}{E_1E_2\Delta} & 0 & 0 & 0 \\ 0 & 0 & 0 & 2G_{23} & 0 & 0 \\ 0 & 0 & 0 & 0 & 2G_{31} & 0 \\ 0 & 0 & 0 & 0 & 0 & 2G_{12} \end{bmatrix}.$$

Material properties are different for each step and incremental stress values are modified according to changes in incremental strains. State dependent mechanical properties are embedded into the ABAQUS with user subroutine UMAT. Material prope (3.7) updated at the beginning of each step. Stresses calculated for each step are added up to find the overall stress level which cause deformation after separation of the tool and the part. In this subroutine, viscous state properties are used for calculating stiffness matrix at the first step. Stress and strains are calculated and stress value is hold in the memory in order use it in the next step. Then, material properties are changed into the rubbery state properties. Stress calculated with the modified properties are added to the stress locked in previous step. For the glassy state, process is going on similarly and overall stresses and strains are calculated [17]. Schematic representation for this process can be seen in Figure 3.2.

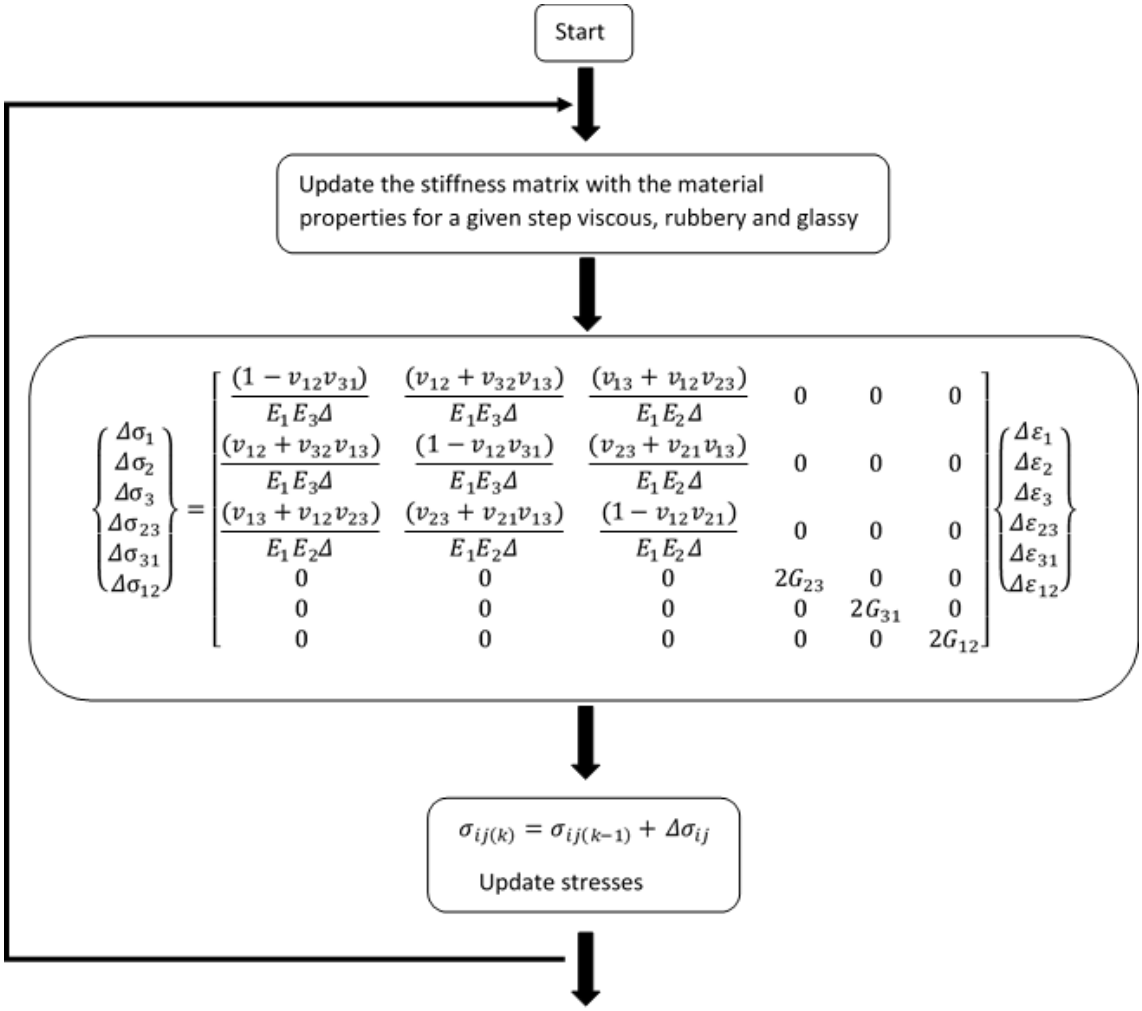


Figure 3.2. Stress calculation progress.

3.2.Steps of Analysis

Chemical structure and physical properties of resin changes during the cure cycle. Cross linking is the main phenomenon that changes the mechanical properties of resin. In the study of Ersoy *et al*. [47], degree of cure is observed as stable at the beginning of the cycle, and then it rises sharply at around the mid portion of second heating ramp. In addition to the degree of cure progress, glass transition temperature which has a similar trend to the degree of cure, increases and goes over the operation temperature at 45 min after the beginning of second hold period. Both situations cause physical changes in the resin. The former one which is called gelation indicate that resin starts to resist shear stress with increasing viscosity. The latter one which is called vitrification indicates that resin starts to

vitrify at that point. Schematic representation of resin property progress along the cure cycle can be seen in Figure 3.3.

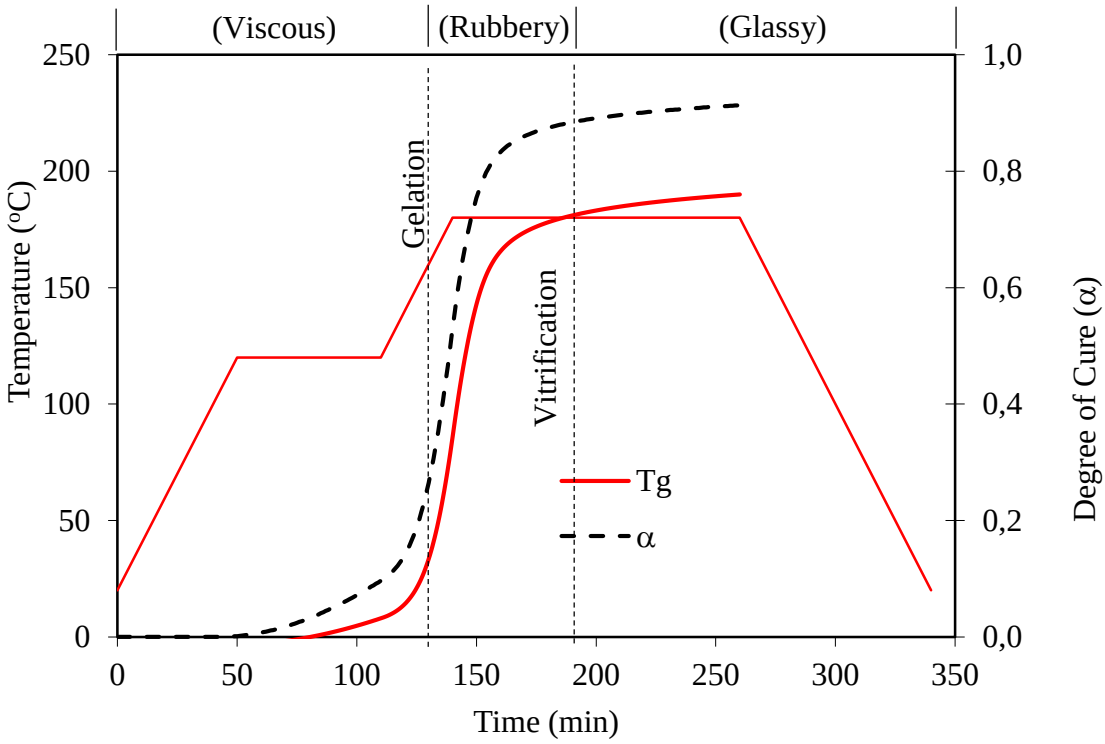


Figure 3.3. Resin property progress through MRCC.

First step of the FEM model simulates the first heating ramp, first temperature hold period and beginning of the second heating ramp in the physical process. At the first part of the cure cycle, degree of cure does not increase in an effective manner; however the temperature hold period is essential for evacuation of voids and bleeding out of extra resin. The first portion of the cure cycle corresponds to the first (viscous) step in ABAQUS model. At this step, the mechanical properties are implemented as a pseudo-viscous manner, in which the shear moduli are taken to be very low, and of-diagonal terms are assumed to be zero in the Jacobian matrix (Equation 3.6) to eliminate cross-interactions. Mechanical properties of resin in this step cannot be obtained by direct methods due to the viscous state of the resin. Çınar *et al*. [56] has performed a parametric study in order to examine the effect of mechanical properties at the first step on final distortion. They assume mechanical

properties of resin in viscous state to be different fractions of the rubbery state properties ($1/5^{th}$ of the rubbery properties).

At the beginning of the second step, degree of cure starts to increase sharply. Together with the degree of cure, crosslinking structure of the thermoset resin increases which causes thickness reduction in the second step. Rubbery state material properties were used in this step in order to model the physical behaviour of resin. At the end of the second step, glass transition temperature reaches the operation temperature and resin vitrifies. After vitrification, resin is solidified at glassy state and has higher elastic modulus than rubbery state. Process induced stresses are locked in the laminate at this state. Mechanical properties for glassy state of the resin are used in this step of analysis. Mechanical properties in different steps of FEM analysis can be seen in Table 3.1.

Table 3.1. Mechanical properties in different steps.

Property	**Unit**	**Viscous**	**Rubbery**	**Glassy**
E11	MPa	132200	132200	135000
E22 = E33	MPa	165	165	9500
G12 = G13	MPa	8.86	44.3	4900
G23	MPa	8.32	41.6	4900
$\nu_{12}=\nu_{13}$	-	0*	0.346	0.3
ν_{23}	-	0*	0.982	0.45
α_{11}	με/°C	0*	0*	0*
$\alpha_{22}=\alpha_{33}$	με/°C	32.6	-320	32.6
$(\varepsilon_{11})^{cure}$	%	0*	0*	0*
$(\varepsilon_{22})^{cure}=(\varepsilon_{33})^{cure}$	%	0*	0.48	0*

*Assumed to be zero

Ersoy *et al*. have studied on mechanical properties of AS4/8552 through MRCC [17, 47] and found the values which can be seen at Table.3.1. by using Group Interaction Modelling to find the mechanical properties of the resin as the cure advances, and micromechanics model to find the mechanical properties of the composites at rubbery and glassy states. Negative CTE for the rubbery state compensates for the cure shrinkage effect

which is experimentally measured as 0.48% in the study of Gartska *et al*. [55]. Due to the constraint caused by fibres, CTE and cure shrinkage in the fibre direction are taken to be zero. Since thin, 4 ply laminates were used in this study, temperature distribution is assumed to be uniform in the laminate.

3.3.Tool-Part Interaction

Tool-part interaction effect was embedded to the ABAQUS model with interaction module. Interaction was created by Surface to Surface Contact (Standard) type. ABAQUS option *SURFACE is used to define the contact surfaces for interactions, then these surfaces are matched by using the option *CONTACT PAIR. The characteristic of the contacting surfaces are defined by using the option *SURFACE BEHAVIOUR. Interaction normal to the surface is the default "hard" contact relationship, which allows no penetration of the slave nodes into the master surface and no transfer of tensile stress across the interface Upper surface of tool was chosen as master surface and tool side surface of laminate was chosen as slave surface. Contact integration property was defined as penalty friction formulation for tangential behaviour. Coulomb friction model is used in order to define the friction mechanism occurring between the tool and the surface. Friction coefficient, μ relate the shear stress to applied pressure up to a limiting stress τ_{max}, at which the two surfaces starts to slide with respect to each other with constant shear stress, as can be seen in Figure 3.4. In the first step, friction coefficient was assumed to be as $\mu = 0.3$ and limiting shear stress to be $\tau_{max}=0.1$. Limiting shear stress was modified to be $\tau_{max} = 0.2$ in the second step. Hard contact relationship does not allow the penetration of slave surface into the master surface and tensile stress is not allowed to transmit between surfaces.

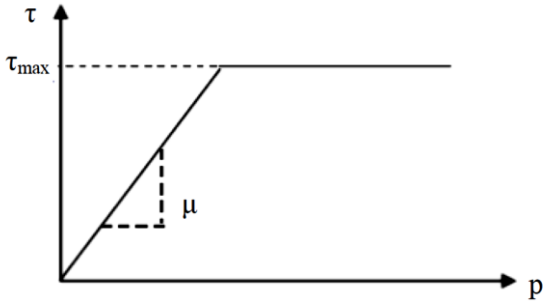


Figure 3.4. Coulomb friction model.

A tool-part interaction phenomenon is one of the main concerns of this study. Strain gages were mounted on samples with spot curing technique. Strain data for the ply attached to the tool has been acquired during the process. Findings exhibit close similarity to the study of Gartska *et al*. [88]. Tool-part interaction exists due to the fibre friction at early stages of cure where the resin is at its viscous state. At the first step, shear stress, which is exerted on the bottom ply, is caused by fibre friction which is in sliding friction mode as found in the study of Ersoy *et al*. [44]. After gelation, interfacial friction turn to be stick-slip friction and tool exerts constant shear on the laminate.

3.4.Meshing and Boundary Conditions

Tools and parts were modelled as quarter models with two symmetry axes. For the tool material, elastic modulus and CTE are defined as 200 GPa and $12.6x10^{-6}$ mm/mm/°C respectively. Reduced quadratic 3D stress elements, which are named as C3D20R, were used for both the tool and the parts. Element sizes are determined with a convergence analysis that can be seen in 3.2-3.3.

Table 3.2. Mesh convergence analysis for double curvature parts.

Double Curvature							
Unidirectional				Cross ply			
Element Type	Seed Size (mm)	Number of Element	Maximum Deformation (mm)	Element Type	Seed Size (mm)	Number of Element	Maximum Deformation (mm)
C3D20R	6	2600	1.278	C3D20R	6	2600	0.9254
C3D20R	5	3720	1.271	C3D20R	5	3720	0.9014
C3D20R	3	10400	1.262	C3D20R	3	10400	0.8623

Table 3.3. Mesh convergence analysis for flat parts.

Plate							
Unidirectional				Cross ply			
Element Type	Seed Size (mm)	Number of Element	Maximum Deformation (mm)	Element Type	Seed Size (mm)	Number of Element	Maximum Deformation (mm)
C3D20R	7.5	1600	0.4680	C3D20R	7.5	1600	0.5362
C3D20R	6	2500	0.4715	C3D20R	6	2500	0.5385
C3D20R	5	3600	0.4734	C3D20R	5	3600	0.5395

Drawing of the whole double curvature mould and symmetry planes can be seen in Figure 3.5. Boundary condition for the bottom surface of the tool is set up to constrain the displacement in the normal direction to the bottom surface. This boundary condition decreases the tool's degree of freedom from 3 to 2. Additionally, symmetric boundary conditions which are defined on symmetry planes, constrain the other degree of freedom. Therefore, midpoint of the tool is fixed in virtual space while boundary conditions allow the tool to expand or contract in any direction without any rotation. Normal contact on tool side surface of part defined in interaction module constrains part in the thickness direction similar to the bottom surface boundary condition defined for the tool. Constraints of symmetry planes can be seen in Table 3.4.

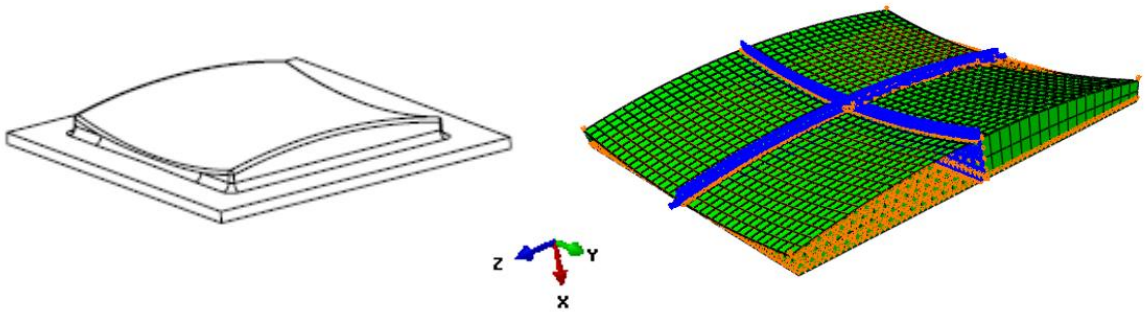


Figure 3.5. Double curvature tool and Symmetric BC's for double curvature tool.

Table 3.4. Constraints for symmetric boundary conditions (X: Fixed).

	Y-symmetry plane	Z-symmetry plane	Bottom plane
U1	-	-	X
U2	X	-	-
U3	-	X	-

In 3D FE model, fibre orientation of individual plies is defined by material orientation. For flat parts, global coordinate system can be used since the geometry allows utilizing rectangular coordinate system. On the other hand, due to the curved geometry of DC tool, global rectangular coordinate system cannot be used to determine material orientation for DC part. ABAQUS provide DISCRETE orientation to define adaptable local coordinate

systems. In discrete coordinate system, users can define local coordinate systems whose one direction can be fixed to the normal of a surface and another direction can be fixed to the edge of geometry. Therefore, discrete type coordinate system was used in order to define material orientation for DC parts. Finally, pressure and temperature changes were defined in ABAQUS. Pressure was applied in the first two steps. In the third step, it was inactivated in order to allow process induced stresses to create deformations without any constraint. Temperature variations were defined with predefined field option.

4. Results and Discussion

Composite parts in different geometries which are chosen to isolate the effect of different mechanisms were manufactured in order to understand the reasons behind process induced residual stresses. Additionally, a Finite Element Model, which includes the effects of tool-part interaction, cure shrinkage and thermal anisotropy, was developed. Distortion fields measured on manufactured parts were compared to Finite Element Model predictions. Therefore, with the help of the experimental measurements of tool-part interaction, isolated effects of different mechanisms can be discussed.

4.1.Tool-Part Interaction

Before curing in the autoclave, prepreg used in the spot curing experiments was tested with INSTRON 8801 tensile testing machine in order to obtain force-strain data to be used in calibration process. Uncured prepreg, on which strain gage was mounted with spot curing, was stretched with constant strain rate. Strain measurement of the gage was calibrated with the strain reading obtained from the video extensometer of the tensile test machine.

At the beginning of the test, a straight portion was observed in the load vs. extension graph which can be explained by the waviness of fibres. Firstly, extension flatten the fibres, then fibres were loaded with tensile stress. This phenomenon was observed in tensile test of uncured prepreg as in Figure 4.1.

Elastic modulus of the uncured prepreg was calculated from Load vs. Strain graph which can be seen in Figure 4.1. Elastic modulus of the prepreg which has a width of 25mm, a length 250mm, and thickness of 0.184 mm was calculated to be 126.125 GPa.

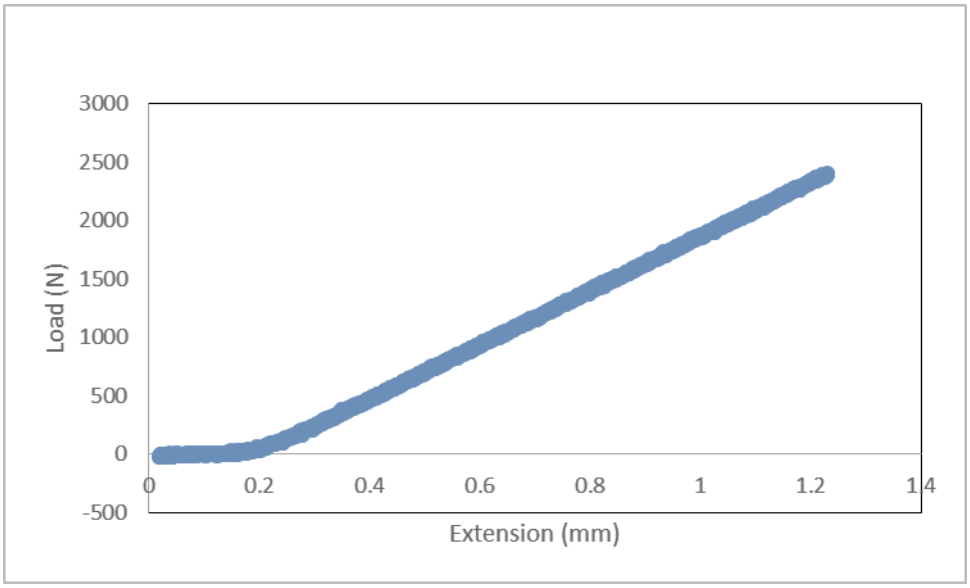


Figure 4.1. Load versus extension data of the uncured prepreg.

Real time raw strain data taken from the spot cured strain gage for the first three hours of the cure cycle could be seen in Figure 4.2. Thermal expansion strain of the tool is superimposed on this strain. The noise in the data is eliminated by a moving average line.

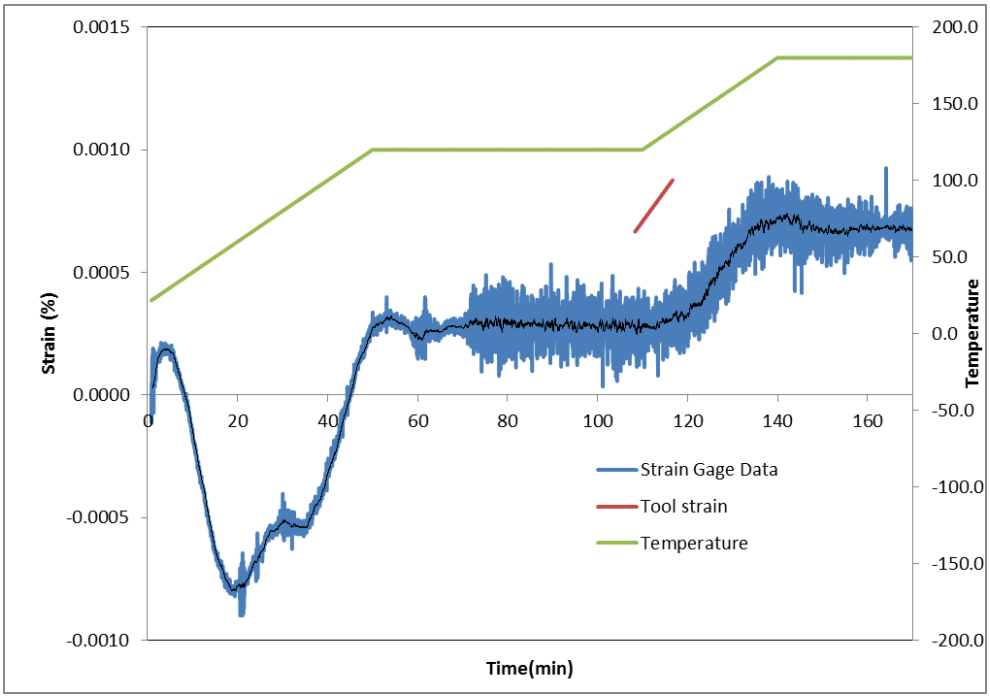


Figure 4.2. Raw data and moving average for real time strain data. (4.1)

At the beginning of the cure cycle, pressure has not reached yet to the set value (7 bar). For the first heat up and temperature hold period, tool-part interaction is caused by friction between fibre and tool surface. Up to the first twenty minutes, there is not any significant shear stress on prepreg due to the unsettled pressure and the wavy fibres in uncured prepreg. However, after the first twenty minutes pressure has reached to a sufficiently high value to create enough friction between tool and part surface. Then, the part was stretched by tool up to the 120 ^{0}C.

Note that, part slipped over the tool at around 30 minutes. Due to the unpredictable behaviour of stick and slip type interaction, it is not possible to develop an exact approach that can predict the overall tool-part interaction behaviour. However, with dozens of experiments and statistical models, prediction errors can be minimized.

Shear stress developed by the tool was calculated with Equation 4.1.

$$\tau = \frac{\varepsilon t E}{L/_2}$$

where ε is calculated from the total strain for sticking period in the first heating ramp which can be seen in Figure 4.2, *t* is thickness of the ply, *E* is elastic modulus in fibre direction for

uncured prepreg and *L* is the length of the part which is equal to 270 mm. Calculated shear stress is equal to 0.172 MPa. Schematic view of the location of the strain gage and the part geometry can be seen in Figure 4.3.

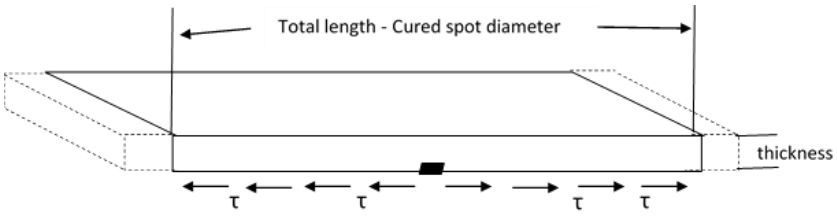


Figure 4.3. Schematic representation for shear stress on bottom ply.

Tool strain at the 2^0C/min temperature ramp and strain gage data can be seen together in Figure 4.2. Parallel trends indicate that there is no relative motion between the part and the tool at the second heating ramp, an observation which also validates the sticking condition.

Shear stress exerted by the tool for the second heating ramp can be calculated by Equation 4.1. Strain value is equal to the 0.0004 % for the second heating ramp which is generated by a shear stress of 0.068 MPa on the tool side surface of the part. Results are similar to the findings of Gartska *et al*. [64] which are shown in Figure 4.4.

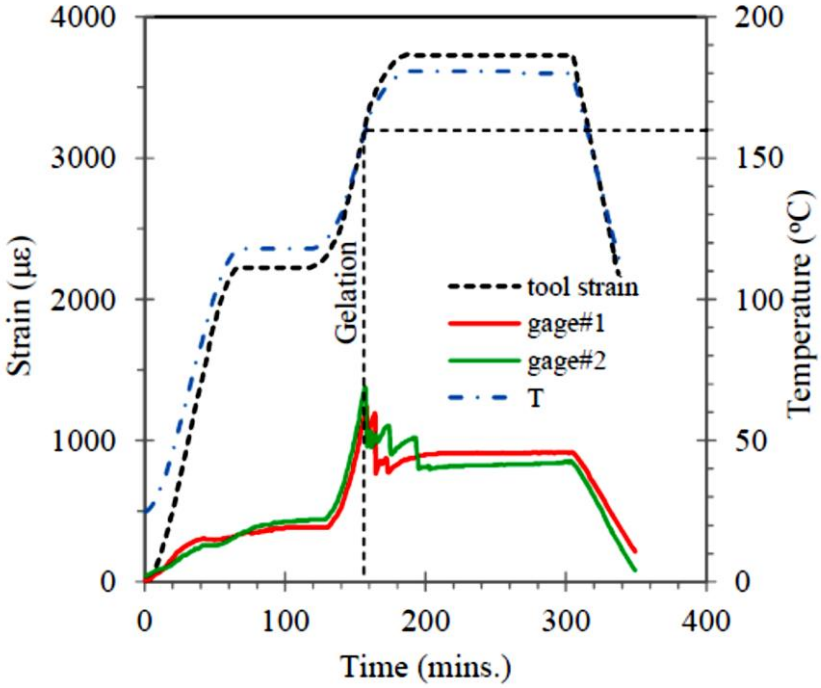


Figure 4.4. Tool-part interaction induced strain [64].

4.2.Comparison of Observed and Predicted Distortion Fields for Flat Plate Parts

A three step 3-D finite element model was developed in order to predict process induced stresses and deformations. Contributions of the thermal expansion anisotropy, cure shrinkage and tool-part interaction on the final process induced stresses were included by the model with user defined material and interaction between the tool and the part. The results of the finite element models were compared to the distortion fields which were obtained from laser scanning of the manufactured parts. Point cloud captured with laser scanning was virtually placed on the tool with three points as can be seen in Figure 4.5. Then fine adjustments were made.



Figure 4.5. Alignment points for tool and scanned data.

For the material coordinate system, 1-direction implies the fibre direction (0°) and 2-direction implies the resin dominated in-plane direction (90°). General material orientation system for the 4-cross-ply laminate can be seen in Figure 4.6.

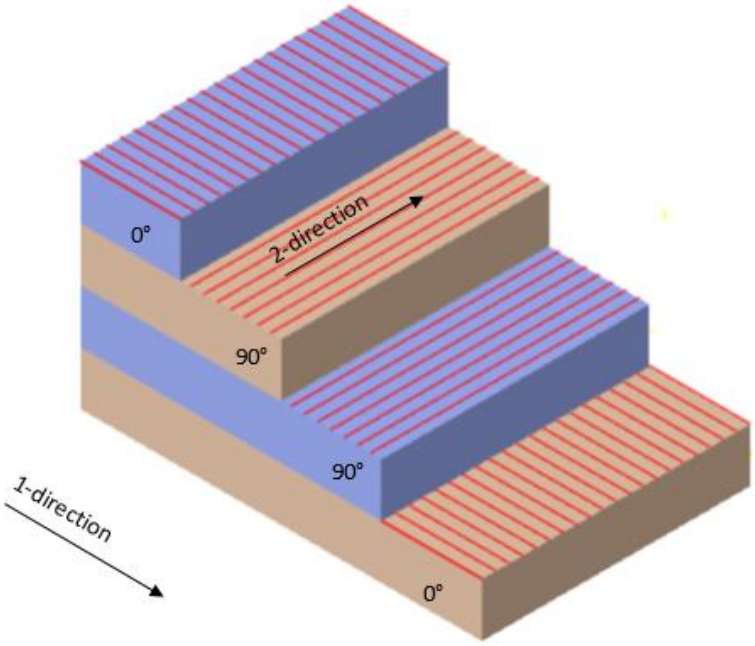


Figure 4.6. Material orientation for the cross-ply laminate.

Three different unidirectional and cross ply laminates were manufactured during this study. Unfortunately, some of the parts are not deformed in predicted manner. The main reason for this situation is fibre misalignment during the lay-up process. Especially for double curvature parts it was really hard to eliminate the fibre misalignment during the lay-up. Effect of fibre misalignment on distortion is not aimed to be investigated in this study, so, the best scan data were selected to be compared to the predicted distortion fields. For comparison between the FEM and measured results, distortion fields for the unidirectional flat parts can be seen in Figures 4.7 and 4.8.

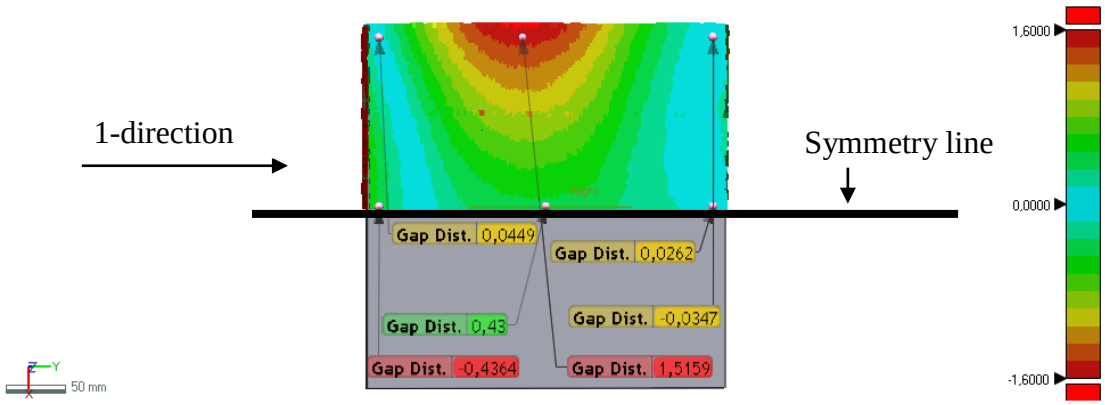


Figure 4.7. Measured distortion field for [0]4 flat part.

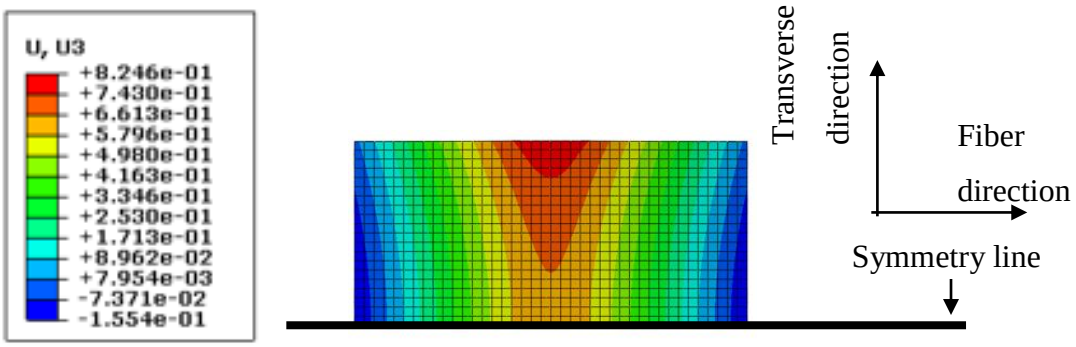


Figure 4.8. Finite element results for [0]4 flat parts.

Fibres close to the tool are stretched more than the fibres away from the tool due to tool-part interaction. Therefore stress gradient occurs in through-thickness direction, which results in concave up warpage in fibre direction. Distortion pattern was captured well by the FE model however there was a difference in the magnitude. Model underestimated the distortion magnitude. Actually, model prediction for distortion pattern at the symmetry line is really precise. However, concave up distortion was higher at the edges than the middle of the part, represented by red colour in Figures 4.7 and 4.8.

Tool-part interaction can be modelled as orthotropic in order to understand the reasons for concave up distortion in transverse direction. If friction coefficient between tool and part is reduced to 10^{-6} in fibre direction while maintaining a value of 0.3 for the transverse direction, finite element model predicts negligible deformation in the laminate. This means that out of plane deformations in transverse direction for UD parts are also caused by tool-

part interaction in fibre direction, because the laminate is very compliant in the transverse direction due to the low modulus in viscous and rubbery steps. Therefore, concave down warpage in transverse direction can be explained by referring to the Poisson's effect. Due to the tool-part interaction, parts are distorted in concave up shape. This warpage cause tensile stress at the outer layers in fibre direction which causes shrinkage of bag side region resin at transverse direction. This approach could be checked in finite element model with variations in Poisson's ratio values for glassy state.

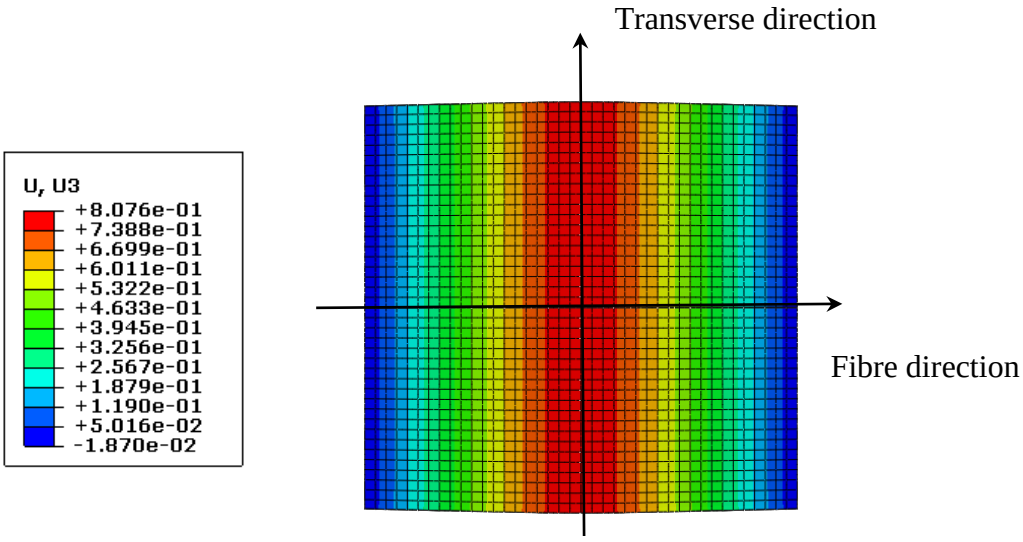


Figure 4.9. Deformation of unidirectional plate without Poisson's ratio effect.

When Poisson's ratio values are set to be equal to zero at glassy state of material, transverse direction deformation does not occur in unidirectional composites parts, and the part deforms to a cylindrical shape, as it can be seen in Figure 4.9. In other words transverse direction concave down warpage in deformation field is caused by Poisson's effect.

Finite element model prediction and measured distortion field are also compared for cross ply laminate in Figures 4.10 and 4.11.

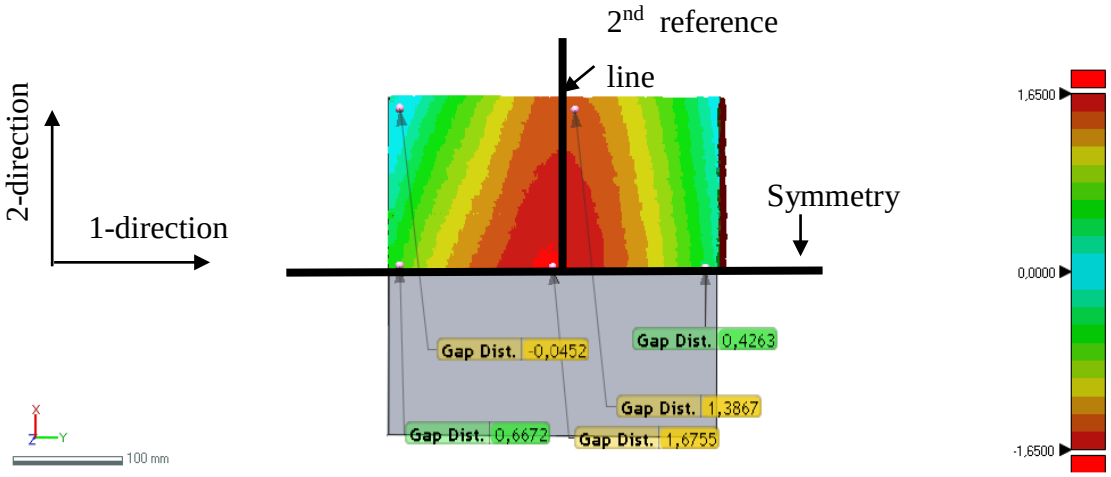


Figure 4.10. Measured distortion field for [0/90]s flat part.

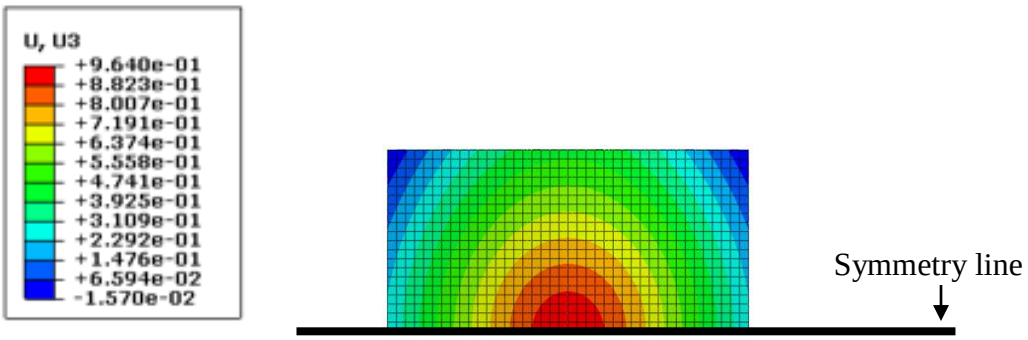


Figure 4.11. Finite element results for [0/90]s flat part.

Distortion fields obtained by measurements on manufactured parts and predicted by the model seem to be similar, so it can be said that the mechanisms behind the process induced residual stresses are well-defined in the numerical study. However, there is a significant difference between magnitudes of numerical and experimental results about the decreasing rate of distortion along the transverse direction from symmetry line to the outer edge. This difference can be explained with the inter-laminar interaction between the first and the second lamina. The tool forces to expand the first lamina in resin dominated direction same as the unidirectional part, however second ply in the cross ply laminate constrain this motion and loaded with tensile stress. Schematic representation can be seen in Figure 4.12.

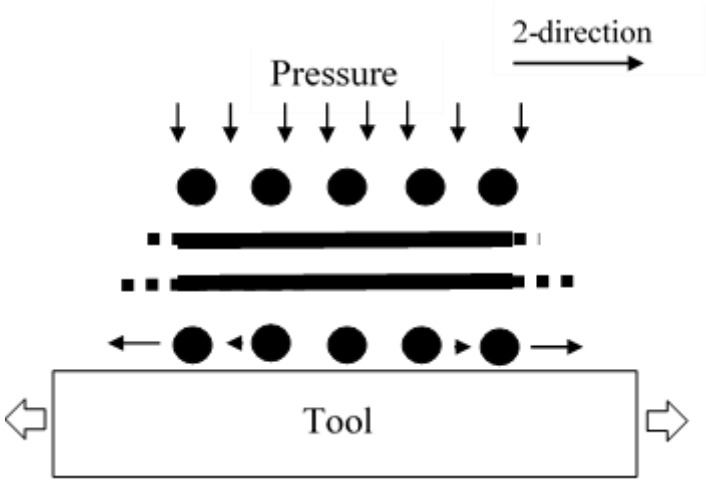


Figure 4.12. Schematic representation of the tool-part interaction in 2-direction.

As well as the interaction between the tool and the part surface, friction may occur between the first and the second ply. In the numerical study, laminate was modelled as a whole body and plies were defined with partition, so second and first plies were attached to each other. This means, for the numerical study, the second ply is loaded in fibre direction (2-direction) with the nearly same stress value as the first ply in its fibre direction (1-direction). So, in the numerical study, different curvatures in 1 and 2-directions are caused basically by difference of the bending stiffness in the two directions due to different distances of the first and the second plies to the neutral axis. In the finite element model, the curvature the 2nd reference line is half of the curvature along the symmetry line, whereas in the actual laminate, the curvature along the 2nd reference line is only one third of the curvature along the symmetry line. This difference can be explained by some other mechanisms that are not taken into account in the model, but causes shear stress loss in the thickness direction, such as inter-laminar friction characteristics, rolling of fibres or the existence of resin rich layer between the fibres of first and second plies.

Asymmetric deformation field can be obtained in numerical study with anisotropic modelling of friction between the tool and the part. Less friction coefficient in transverse direction cause less stress on the second ply in transverse direction which is second ply's fibre direction. In ABAQUS, ANISOTROPIC option for *FRICTION allows one to define different friction coefficients for fibre and transverse directions. So reduced friction coefficient in transverse direction simulate the shear loss phenomena between tool and

second ply. Distortion field for a friction coefficient of 0.15 in transverse direction can be seen in Figure 4.13. Friction coefficient in fibre direction is kept to be 0.3 as in other models.

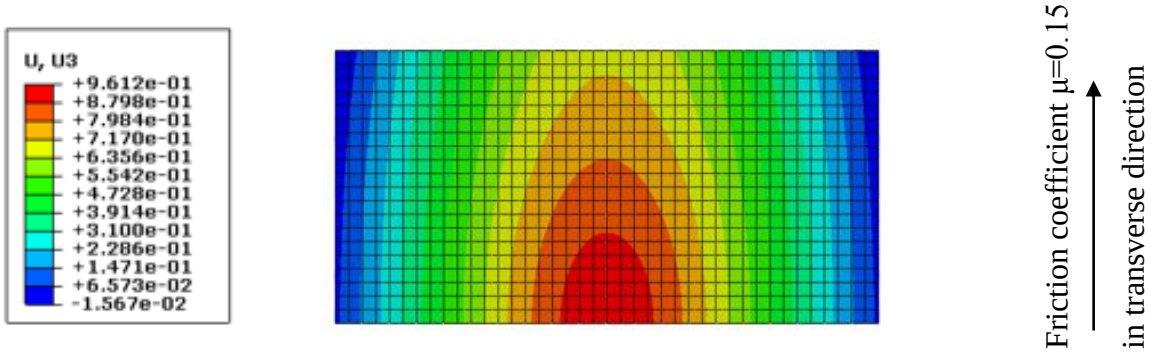


Figure 4.13. Modified distortion field with reduced transverse direction friction coefficient.

4.3.Comparison of Observed and Predicted Distortion Fields for Double Curvature Parts

Three step 3-D finite element model which includes thermal expansion anisotropy, cure shrinkage, consolidation, and tool-part interaction was implemented in order to predict process induced stresses and deformations in double curvature parts. The main difference of this geometry from the flat part is the contribution of cure shrinkage and thermal anisotropy into the overall distortion field due to the curved geometry.

Distortion fields predicted by FEM and measured from manufactured part can be seen in Figures 4.14 and 4.15 for unidirectional double curvature parts. Note that negative values for Finite Element Model results imply concave up deformation similar to the actual deformation field. They are negative due to the coordinate system.

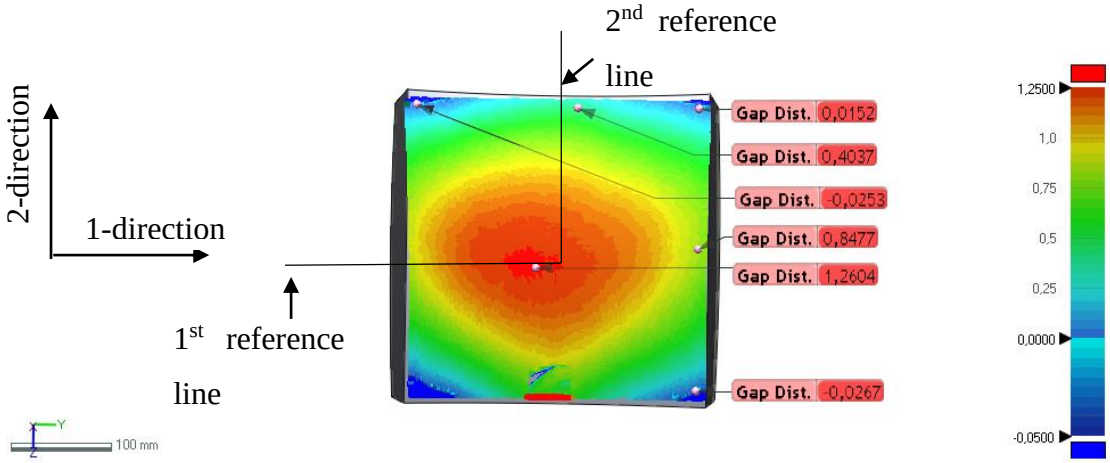


Figure 4.14. Measured distortion field for [0]4 double curvature part.

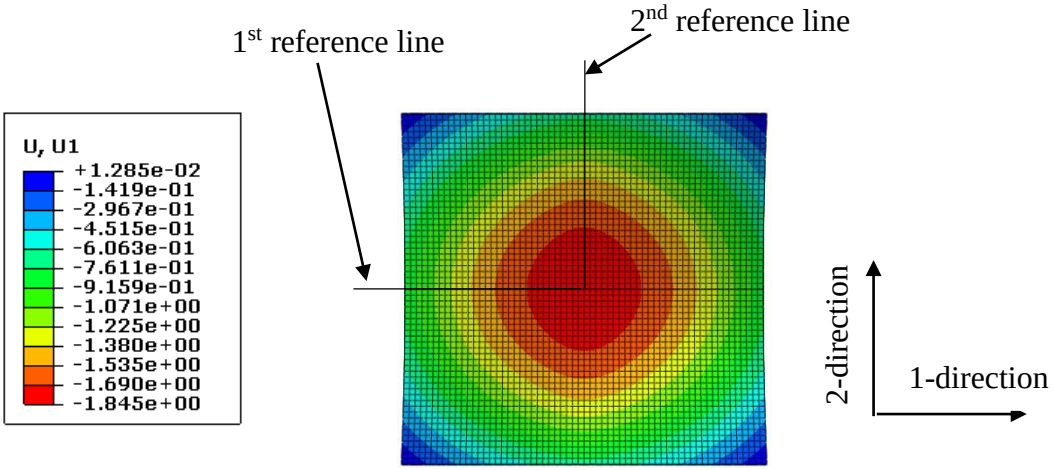


Figure 4.15. Finite element results for [0]4 double curvature part.

The measured distortion field for double curvature unidirectional part is very close to the finite element result. The finite element model gives more precise distortion field predictions as compared to the flat part. In fibre direction, tool-part interaction creates the concave up warpage as similar to the flat part. However, different mechanisms like cure shrinkage and thermal anisotropy, which are not effective in flat geometry, contribute to shape distortions in this geometry. In the 1-direction, concave up curvature of the part increases the concave up curvature due to the mechanisms of thermal anisotropy and cure shrinkage which generate spring-in effect. Cumulative distortional effect of different mechanisms that act in the same direction can be seen schematically in Figure 4.16.

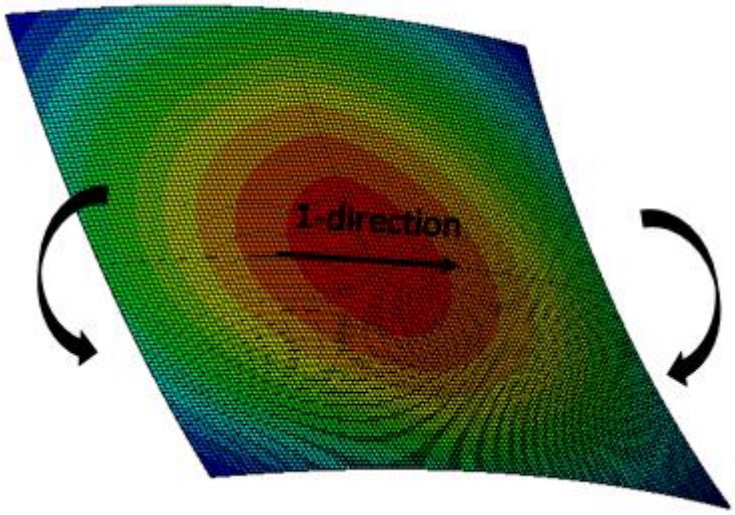


Figure 4.16. Cumulative spring in effect of thermal anisotropy, cure shrinkage and tool-part interaction.

In order to understand the contribution of various mechanisms on overall distortion, the effect of cure shrinkage, thermal anisotropy, and tool-part interaction can be isolated in the finite element model. The effect of cure shrinkage and thermal anisotropy can be suppressed by setting the coefficient of thermal expansions in Step-1 and Step-2 to be zero.

Maximum distortion value for the double curvature plate is equal to the 1.845 mm for the model including all of the mechanisms. Elimination of the cure shrinkage decreases maximum distortion by 0.256 mm and elimination of the thermal coefficient effect decreases maximum distortion by 0.221 mm. Therefore, it can be concluded that main contributor to the deformation is the tool-part interaction mechanism.

Distortion fields for cross-ply double curvature parts predicted by FEM and measured from manufactured part can be seen in Figures 4.17 and 4.18. Finite Element results are negative due to the coordinate system, so colour representation for actual case and numerical study express same side of deformation.

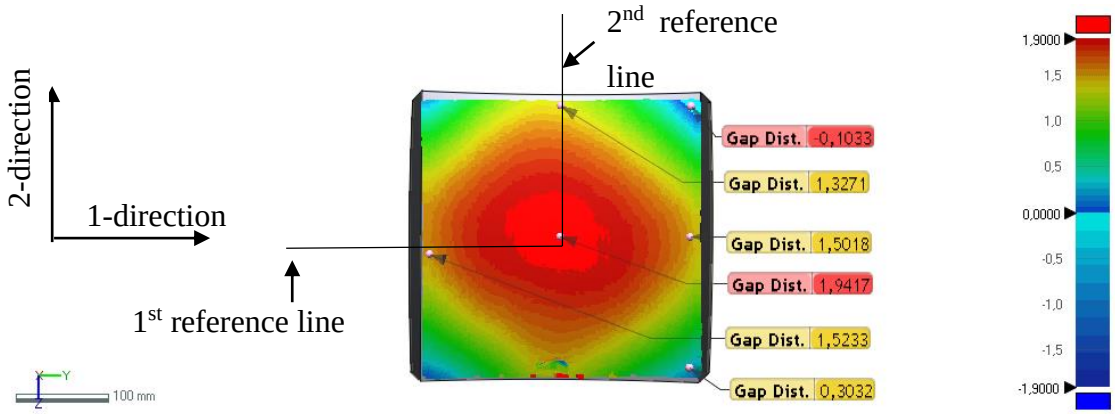


Figure 4.17. Measured distortion field for [0/90]s double curvature part.

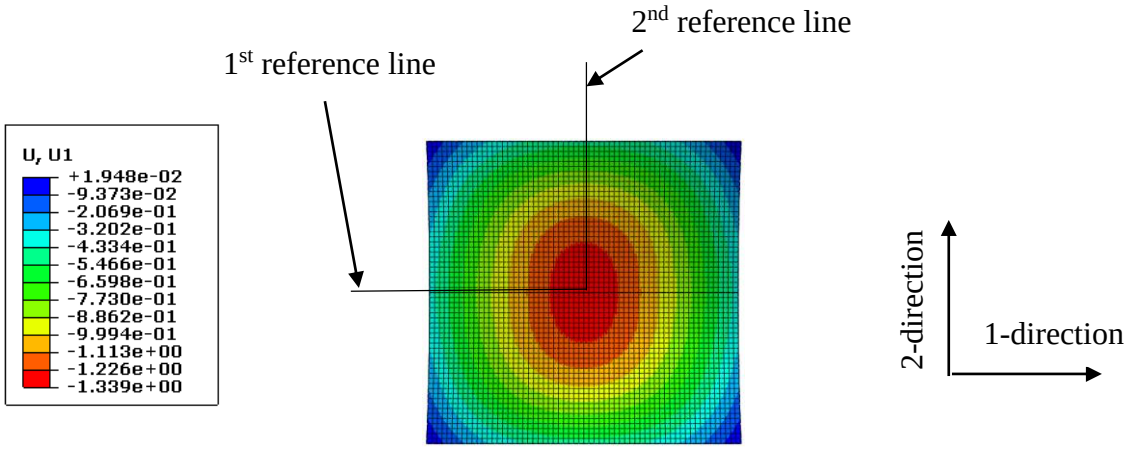


Figure 4.18. Finite element results for [0/90]s double curvature part.

A closer look to the deformation values reveals that finite element model overestimates the distortion field along the first reference line.

The maximum deformation is 1.339 mm and suppressing the cure shrinkage and thermal anisotropy effects decreases the maximum deformation. Cure shrinkage contribution to the maximum deformation is found to be 0.180 mm and thermal anisotropy contribution to be 0.090 mm.

For the cross ply laminate, predictions including cure shrinkage and thermal anisotropy effects are more accurate for the second reference line whereas deformation along the first reference line is overestimated in the same manner as the flat parts. This phenomenon can be explained by shear loss along the through-the-thickness direction. Therefore, friction

behaviour is modified to be anisotropic with a friction coefficient of 0.15 along 2nd reference line whereas maintaining a friction coefficient of 0.3 along 1st reference line. The resulting deformation field can be seen in Figure 4.19. Modifying the friction coefficients in two directions by using an anisotropic friction model enables the model to capture different curvatures in two directions.

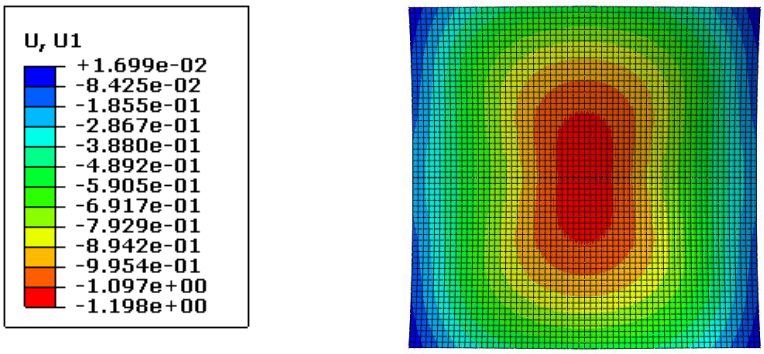


Figure 4.19. Anisotropic friction coefficient for double curvature cross ply laminate.

5. Conclusion and Future Works

Double curvature and flat parts are manufactured to examine the effects of various mechanisms contributing to distortion and process induced residual stresses. Additionally, 3D finite element models have been developed to predict the distortion patterns of these parts. Measured distortion patterns are compared to the predicted ones. Tool-part interaction approach used in numerical study is verified with strain data acquired by a spot cured strain gage on an uncured prepreg which is then processed on a flat tool in the autoclave by using conventional bagging and process conditions.

The main results of this study are as follows:

The finite element model which simulates processing of composite parts in the autoclave captures the distortion fields reasonably well, however it includes many process and material parameters, so the effect of various parameters should be analysed by a parametric study to refine the predictions. Parameters such as shear moduli and friction coefficients should be fine-tuned in order to have more accurate predictions.

Unidirectional flat plates deform in a concave up shape in the fibre direction, and concave down shape in transverse direction and this is explained with the Poisson's effect. Fibre direction comparisons reveal that model predictions are well matched with actual case.

The most important result of cross ply flat laminate is to observe shear loss phenomena between tool and the second ply. This phenomenon may be explained with the sliding interaction between the first and the second ply or fibre rolling in the first ply, which is not included in the model. Anisotropic friction definition between the tool and the part show that if shear stress is reduced in transverse direction, deformation fields obtained by actual measurements and numerical predictions are converging.

The relative effects of cure shrinkage, thermal anisotropy and tool-part interaction is examined by selectively suppressing individual effects in the model. It has been found that main contributor to the deformation is tool-part interaction.

Distortion field prediction for cross ply double curvature parts can be refined by using anisotropic friction coefficients, however, the actual friction coefficients in both fibre and

transverse directions should be measured by using appropriate techniques. In this study, only frictional characteristics of the prepregs against the tool are measured only in the fibre direction.

Tool-part interaction measurements using spot curing technique prove that sticking condition prevails throughout the whole cure cycle, although during the first heating ramp in which resin is in its viscous state, some slipping motion is observed.

The following points are suggested to be investigated in more detail in a future work in order to have a better understanding of the nature of tool-part interaction in composites manufacturing:

Shear stress distribution along the through-thickness direction is essential to examine the process induced residual stresses and their effects on final shape distortions resulting from manufacturing processing of composite materials. Shear distribution along the thickness direction and shear modulus which determines how shear stress transfer from tool-side ply to bag-side ply should be measured with multiple strain gages mounted on different plies of the laminate.

Interlaminar interactions especially between the first and the second plies may be included in the model and experimentally measured using multiple strain gages mounted on every layer.

Lay-up process and fibre alignment are crucially effective on the final distortion pattern. A parametric study may be developed to predict final distortion variance for inevitable fibre misalignments.

Resin percolation phenomenon may also be included to the numerical model in order to examine the effect of Fibre Volume Fraction gradients occurring in bleeding prepreg systems.

The main contribution of this study to the existing body of knowledge on manufacturing deformations of composite parts is the observations and predictions made on two-dimensional flat and curved parts. Effect of tool-part interaction is only investigated using flat strips in the literature, and the effect of tool-part interaction in the transverse direction is not very well understood so far. The findings in this study show that the tool-

part interactions in the fibre and transverse directions are the main contributors to distortion, and the model developed captures basic features of deformation patterns. However, more detailed measurements on tool-part interactions should be performed to fine-tune the predictive finite element model.

REFERENCES

1. Mazumdar, S.K., *Composites Manufacturing*, CRC Press, Florida, 2002.

2. Sarrazin, H., B. Kim, S.H. Ahn, and G.S. Springer, "Effects of Processing Temperature and Lay-up on Springback", *Journal of Composite Materials,* Vol. 29, No. 10, pp. 1278-1294, 1995.

3. Gigliotti, M., M.R. Wisnom, and K.D. Potter, "Development of Curvature during the Cure of AS4/8552 [0/90] Unsymmetric Composite Plates", *Composite Science and Technology*, Vol. 63, No. 2, pp. 187-197, 2003.

4. Svanberg, J.M., and J.A. Holmberg, "An Experimental Investigation on Mechanisms for Manufacturing Induced Shape Distortions in Homogeneous and Balanced Laminates", *Composites Part A,* Vol. 32, No. 6, pp. 827–838, 2001.

5. Ersoy, N., K., Potter, M.R. Wisnom, and M.J. Clegg, "Development of Spring-in Angle during Cure of a Thermosetting Composite", *Composites Part A,* Vol. 36, No. 12, pp. 1700-1706, 2005.

6. Radford, D.W., and T.S. Rennick, "Separating Sources of Manufacturing Distortion in Laminated Composites", *Journal of Reinforced Plastics and Composites*, Vol. 19, No. 8, pp. 621-640, 2000.

7. Garstka, T., *Separation of Process Induced Distortions in Curved Composite Laminates*, Ph.D. Thesis, University of Bristol, 2005.

8. Derek Hull, *An Introduction to Composite Materials*, Cambridge University Press, New York, 1981.

9. Radford, D.W., and R.J. Diendorf, "Shape Instabilities in Composites Resulting from Laminate Anisotropy", *Journal of Reinforced Plastics and Composites,* Vol. 12, No. 1, pp. 58-75, 1993.

10. White, S.R., and H.T. Hahn, "Process Modelling of Composite Materials: Residual Stress Development during Cure. Part II. Experimental Validation", *Journal of Composite Materials,* Vol. 26, No. 16, pp. 2423-2453, 1992.

11. Russell, J.D., M.S. Madhukar, MS. Genidy, and A.Y. Lee, "A New Method to Reduce Cure-Induced Stresses in Thermoset Polymer Composites, Part III: Correlating Stress History to Viscosity, Degree of Cure, and Cure Shrinkage", *Journal of Composite Materials,* Vol. 34, No. 22, pp. 1926-1947, 2000.

12. Msallem, Y.A., F. Jacquemin, N. Boyard, A. Poitou, D. Delaunay, and S. Chatel, "Material Characterization and Residual Stresses Simulation during the Manufacturing Process of Epoxy Matrix Composites", *Composites Part A,* Vol. 41, No. 1, pp. 108-115, 2010.

13. Prasatya, P., G.B. McKenna, and S.L. Simon, "A Viscoelastic Model for Predicting Isotropic Residual Stresses in Thermosetting Materials: Effects of Processing Parameters", *Journal of Composite Materials,* Vol. 35, No. 10, pp. 826-847, 2001.

14. Madhukar, M.S., MS. Genidy, and J.D. Russell, "A New Method to Reduce Cure-Induced Stresses in Thermoset Polymer Composites, Part I:Test Method", *Journal of Composite Materials,* Vol. 34, No. 22, pp. 1882-1904, 2000.

15. Johnston, A., *An Integrated Model of the Development of Process-induced Deformation in Autoclave Processing of Composite Structures,* Ph.D. Thesis, The University of British Columbia, 1997.

16. Ersoy, N., and M. Tugutlu, "Cure Kinetics Modelling and Cure Shrinkage Behaviour of a Thermosetting Composite", *Polymer Engineering and Science,* Vol. 50, No. 1, pp. 84-92, 2010.

17. Ersoy, N., T. Garstka, K. Potter, and M.R. Wisnom, D. Porter, and G. Stringer, "Modelling of the Spring-in Phenomenon in Curved Parts Made of a Thermosetting Composite", *Composite Part A,* Vol. 41, No. 3, pp. 410-418, 2010.

18. Wisnom M.R., N. Ersoy, and K.D. Potter "Shear-lag analysis of the effect of thickness on spring-in of curved composites", *Journal of Composite Materials,* Vol. 41, No. 11, pp. 1311–24, 2007.

19. Hubert, P., and A. Poursartip, "A Review of Flow and Compaction Modelling Relevant to Thermoset Matrix Laminate Processing", *Journal of Composite Materials,* Vol. 17, No. 4, pp. 286-318, 1998.

20. Dave, R., JL. Kardos, and M P. Dudukovic, “A Model for resin flow during Composite Processing: Part 1-General Mathematical Development”, *Polymer Composites*, Vol. 8, No. 1, pp. 29-38, 1987.

21. Gutowski, T G., Z. Cai, S. Bauer, and D. Boucher, “Consolidation Experiments for Laminate Composites”, *Journal of Composite Materials*, Vol. 21, No. 7, pp. 650-669, 1987.

22. Hubert, P., R. Vaziri, and A. Poursartip “A Two-Dimensional Flow Model for the Process Simulation of Complex Shape Composite Laminates”, *International Journal for Numerical Methods in Engineering*, Vol. 44, No. 1, pp. 1-26, 1999.

23. Li, M., Y. Li, Z. Zhang, and Y. Gu, “Numerical Simulation Flow and Compaction during the Consolidation of Laminated Composites”, *Polymer Composites*, Vol. 29, No. 5, pp. 560-568, 2008.

24. Li, M., L. Charles, and III., Tucker, “Modelling and Simulation of Two-dimensional Consolidation for Thermoset Matrix Composites”, *Composites Part A*, Vol. 33, No. 6, pp. 877-892, 2002.

25. Dong, C.S., “Model Development for the Formation of Resin-rich Zones in Composites Processing”, *Composites Part A*, Vol. 42, No. 4, pp. 419-424, 2011.

26. Radford, D.W., “Cure Shrinkage-induced Warpage in Flat Uniaxial Composites”, *Journal of Composites Technology and Research*, Vol. 15, No. 4, pp. 290-296, 1993.

27. Prasatya, P., G.B. McKenna, and S.L. Simon, “A Viscoelastic Model for Predicting Isotropic Residual Stresses in Thermosetting Materials: Effects of Processing Parameters”, *Journal of Composite Materials*, Vol. 35, No. 10, pp. 826-847, 2001.

28. Twigg, G., A. Poursartip, and G. Ferlund, “An Experimental Method for Quantifying Tool-part Shear Interaction during Composites Processing”, *Composite Science and Technology*, Vol. 63, No. 13, pp. 1985-2002, 2003.

29. Twigg, G., A. Poursartip, and G. Ferlund, “Tool-part Interaction in Composite Processing. Part I: Experimental Investigation and Analytical Model”, *Composite Part A*, Vol. 35, No. 1, pp. 121-133, 2004.

30. Twigg, G., A. Poursartip, and G. Ferlund, “Tool-part Interaction in Composite Processing. Part II: Numerical Modelling”, *Composite Part A*, Vol. 35, No. 1, pp. 135-141, 2004.

31. Potter, K.D., M. Campbell, C. Langer, and M.R. Wisnom "The Generation of Geometrical Deformations due to Tool/Part interaction in the Manufacture of Composite Components", *Composite Part A*, Vol. 36, No. 2, pp. 301-308, 2005.

32. Stefaniak, D., E. Kappel, T. Sprowitz, and C. Hühne, "A Semi-analytical Simulation Strategy and its Application to Warpage of Autoclave-processed CFRP Parts", *Composite Part A*, Vol.42, No. 12, pp. 1985-1994, 2011.

33. Stefaniak, D., E. Kappel, T. Sprowitz, and C. Hühne, "Experimental Identification of Process Parameters Inducing Warpage of Autoclave-processed CFRP Parts", *Composite Part A*, Vol. 43, No. 7, pp. 1081-1091, 2012.

34. Özsoy, Ö.Ö., N. Ersoy, and M.R. Wisnom, "Numerical Investigation of Tool-part Interactions in Composite Manufacturing", *Proceedings of ICCM-16, 16th International Conference on Composite Materials*, 2007.

35. Zeng, X., and J. Raghavan, "Role of Tool-part Interaction in Process-Induced Warpage of Autoclave-Manufactured Composite Structures", *Composite Part A*, Vol. 41, No. 9, pp. 1174-1183, 2010.

36. Kaushik, V., and J. Raghavan, "Experimental Study of Tool-part Interaction during Autoclave Processing of Thermoset Polymer Composite Structures", *Composite Part A*, Vol. 41, No. 9, pp. 1210-1218, 2010.

37. Arafath, A.R.A., R. Vaziri, and A. Poursartip, "Closed-form Solution for Process-induced Stresses and Deformation of a Composite Part Cured on a Solid Tool: Part I- Flat Geometries", *Composite Part A*, Vol. 39, No. 7, pp. 1106-1117, 2008.

38. Arafath, A.R.A., R. Vaziri, and A. Poursartip, "Closed-form Solution for Process-induced Stresses and Deformation of a Composite Part Cured on a Solid Tool: Part I- Curved Geometries", *Composite Part A*, Vol. 40, No. 10, pp. 1545-1557, 2009.

39. de Oliveria, R., S. Lavanchy, R. Chatton, D. Costantini, V. Michaud, R. Salathe, and J.A.E. Manson, "Experimental Investigation of the Mould Thermal Expansion on the Development of Internal Stresses during Carbon Fibre Composite Processing", *Composite Part A*, Vol.39, No. 7, pp. 1083-1090, 2008.

40. Ferlund, G., N. Rahman, R. Courdji, M. Bresslauer, A. Poursartip, K. Willden and K. Nelson, "Experimental and Numerical Study of the Effect of Cure Cycle, Tool Surface,

Geometry, and Lay-up on the Dimensional Fidelity of Autoclave-processed Composite Parts", *Composite Part A*, Vol. 33, No. 3, pp. 341-351, 2002.

41. Zhu, Q., P.H. Geubelle, M. Li, C.L.III Tucker, "Dimensional Accuracy of Thermoset Composites: Simulation of Process-induced Residual Stresses", *Journal of Composite Materials*, Vol. 35, No. 24, pp. 2171-2205, 2001.

42. Flanagan, R., *The Dimensional Stability of Composite Laminates and Structures*, Ph.D. Thesis, Queen's University of Belfast, 1997.

43. Martin, C.J., J.C. Seferis, and M.A. Wilhelm, "Frictional Resistance of Thermoset Prepregs and its Influence on Honeycomb Composite Processing", *Composites Part A*, Vol. 27, No. 10, pp. 943–951, 1996.

44. Ersoy, N., K. Potter M.R. Wisnom and M.J. Clegg "An Experimental Method to Study Frictional Processes During Composite Manufacturing", *Composites Part A*, Vol. 36, No. 11, pp. 1536–1544, 2005.

45. Johnston, A., R. Vaziri, and A. Poursartip, "A Plane Strain Model for Process-induced Deformation of Laminated Composite Structures", *Journal of Composite Materials*, Vol. 35, No. 16, pp. 1435-1469, 2001.

46. Khoun, L., and P. Hubert, "Investigation of the Dimensional Stability of Carbon Epoxy Cylinders Manufactured by Resin Transfer Moulding", *Composites: Part A*, Vol. 41, No. 1, pp. 116-124, 2010.

47. Ersoy N., *et al*. "Development of the properties of a carbon fibre reinforced thermosetting composite through cure", *Composites: Part A*, Vol. 41, No. 3, pp. 401–9, 2010.

48. Hahn, H.T., and N.J. Pagano, "Curing Stresses in Composite Laminates", *Journal of Composite Materials*, Vol. 9, No. 1, pp. 9-91, 1975.

49. Bogetti, T.A., and JR. J.W. Gillespie "Process-induced Stress and Deformation in Thick-section Thermoset Composite Laminates", *Journal of Composite Materials*, Vol. 26, No. 5, pp. 626-660, 1992.

50. Loos, A.C., and G.S. Springer, "Curing of Epoxy Matrix Composites", *Journal of Composite Materials*, Vol. 17, No. 2, pp. 135-169, 1983.

51. Huang, C.K., and S.Y. Yang, "Warping in Advanced Composite Tools with Varying Angles and Radii.", *Composites: Part A*, Vol. 28, No. 9, pp. 891-893, 1997.

52. Salomi, A., T. Garstka, K. Potter, A. Greco, and A. Maffezzoli, "Spring-in Angle as Moulding Distortion for Thermoplastic Matrix Composite", *Composite Science and Technology*, Vol. 68, No. 14, pp. 3047-3054, 2008.

53. Yoon, K.J., and J.S. Kim, "Effect of Thermal Deformation and Chemical Shrinkage on the Process Induced Distortion of Carbon/Epoxy Curved Laminates", *Journal of Composite Materials*, Vol. 35, No. 3, pp. 253-263 2001.

54. Min, L., L. Yanxia, and G. Yizhuo, "Numerical Simulation Flow and Compaction during the Consolidation of Laminated Composites", *Wiley Interscience, Society of Plastic Engineers*, Vol. 29, No. 5, pp. 560-568, 2008.

55. Garstka, T., N. Ersoy, K. Potter, and M.R. Wisnom, "In Situ Measurements of Through-the-Thickness Strains during Processing of AS4/8552 Composite", *Composites: Part A*, Vol. 38, No. 12, pp. 2517–2526, 2007.

56. Çınar, K., *Process Modelling for Distortions in Manufacturing of Fibre Reinforced Composite Materials*, Ph.D. Thesis, Boğaziçi University, 2014.

57. Svanberg, J.M., and J.A. Holmberg, "Prediction of Shape Distortions. Part II. Experimental Validation and Analysis of Boundary Conditions", *Composites: Part A*, Vol. 35, No. 6, pp. 723-734, 2004.

58. Bogetti, T., A., and J. W. Gillipse, "Processing-Induced Stress and deformation in Thick Section Thermosetting Composite Laminates", CCM Report 89-21, University of Delaware, August, 1989.

59. Lightfoot, S.C., M.R. Wisnom, and K. Potter, "A New Mechanism for the Formation of Ply Wrinkles due to Shear between Plies", *Composites Part A*, Vol. 49, pp. 139-147, 2013.

60. Potter, K., C. Langer, B. Hodgkiss, and S. Lamb, "Sources of Variability in Uncured Aerospace Grade Unidirectional Carbon Fibre Epoxy Preimpregnate", *Composites: Part A*, Vol. 38, No. 3, pp. 905-916, 2007.

61. de Oliveria, R., S. Lavanchy, R. Chatton, D. Costantini, V. Michaud, R. Salathe, and J.A.E. Manson, "Experimental Investigation of the Mould Thermal Expansion on the Development of Internal Stresses during Carbon Fibre Composite Processing", *Composite Part A*, Vol.39, No. 7, pp. 1083-1090, 2008.

62. Kim, Y.K., and I.M. Daniel, “Cure Cycle Effect on Composite Structures Manufactured by Resin Transfer Moulding”, *Journal of Composite Materials*, Vol. 36, No. 14, pp. 1725-1742, 2002.

63. Antonucci, V., A. Cusano, M. Giordano, J. Nasser, and L. Nicolais, “Cure- induced Residual Strain Build-up in a Thermoset Resin”, *Composites Part A*, Vol. 37, No. 4, pp. 592-601, 2006.

64. Garstka, T., N. Ersoy, K. Potter, and M.R. Wisnom, “Observations on Tool-Part Interaction in Curved Composite Parts”, *Journal of Composite Materials,* under review, 2012